



Minnesota State University, Mankato
Cornerstone: A Collection of Scholarly
and Creative Works for Minnesota
State University, Mankato

All Graduate Theses, Dissertations, and Other
Capstone Projects

Graduate Theses, Dissertations, and Other
Capstone Projects

2020

Control of a Grid-Tied Single-Phase Inverter for Renewable Energy Integration

Dianzhi Yu
Minnesota State University, Mankato

Follow this and additional works at: <https://cornerstone.lib.mnsu.edu/etds>

 Part of the [Controls and Control Theory Commons](#), and the [Power and Energy Commons](#)

Recommended Citation

Yu, D. (2020). Control of a grid-tied single-phase inverter for renewable energy integration [Master's thesis, Minnesota State University, Mankato]. Cornerstone: A Collection of Scholarly and Creative Works for Minnesota State University, Mankato. <https://cornerstone.lib.mnsu.edu/etds/1068/>

This Thesis is brought to you for free and open access by the Graduate Theses, Dissertations, and Other Capstone Projects at Cornerstone: A Collection of Scholarly and Creative Works for Minnesota State University, Mankato. It has been accepted for inclusion in All Graduate Theses, Dissertations, and Other Capstone Projects by an authorized administrator of Cornerstone: A Collection of Scholarly and Creative Works for Minnesota State University, Mankato.

CONTROL OF A GRID-TIED SINGLE-PHASE INVERTER FOR RENEWABLE
ENERGY INTEGRATION

by

Dianzhi Yu

A THESIS

submitted in partial fulfillment of the requirements
for the degree of Master Science in Electrical Engineering
at Minnesota State University, Mankato

Major: Electrical Engineering

Under the Supervision of Professor Jianwu Zeng

Mankato, Minnesota

July, 2020

July 10, 2020

CONTROL OF A Grid-TIED SINGLE-PHASE INVERTER FOR RENEWABLE
ENERGY INTEGRATION

Dianzhi Yu

This thesis has been examined and approved by the following members of the student's
committee.

Advisor

Committee Member

Committee Member

CONTROL OF A GRID-TIED SINGLE-PHASE INVERTER FOR RENEWABLE ENERGY INTEGRATION

Dianzhi Yu, M.S.

Minnesota State University, Mankato, 2020

Advisor: Jianwu Zeng

With increasing demand for generating electricity from clean energy, renewable energy sources (RESs), such as wind and solar, has gained much attention due to the clean and quiet characteristics. In many applications, connecting multiple RESs of different types (e.g., wind and solar), voltages, and capacities to a power grid or load is required. Single-phase inverters have been widely installed in residential power system to meet the full or partial load demand.

In this work, multiport converters were developed for integrating multiple RESs, wind turbine and photovoltaic (PV) panel. Since the intermittent characteristic of the RESs, an energy storage device, e.g., batteries, needs to be used together. First, multiport DC-DC converters were proposed for simultaneous maximum power point tracking (MPPT) control of each source. However, the output of these converters is DC and cannot be directly connected to the AC utility grid which requires a DC-AC inverter regulates the voltage from DC to AC. This thesis introduces a single-phase, four-port inverter for integrating RESs to the AC utility grid. All controllers are developed in rotation d-q frame. The inverter not only can operate in a standalone mode, but also can works with other inverters with the droop control as well as the grid.

ACKNOWLEDGMENTS

I would like to express my appreciation and thanks to my advisor, Dr. Jianwu Zeng, for all the substantial support, patient instructions, insightful discussions and tremendous assistance for my study and research. He is an enthusiastic researcher with critical thinking and rich experience, who sets an excellent example for me. He has given me many valuable opportunities that help me learn. His advice is helpful not only for my study, but also for my career.

In addition, I would like to thank my thesis committee, Dr. Qun Zhang and Dr. Vincent Winstead for their suggestions and comments on my thesis research as well as their assistance throughout the process of my master work.

I am grateful to my group members Xia Du, Jiahong Ning, Zhaoxia Yang and Ramkrishna Mishan. Thank you for sharing their experiences in building up the experiments and adhesive studying atmosphere. Financial support from the Xcel Energy through a grant from the Renewable Development Fund is gratefully acknowledged.

Furthermore, I appreciate Dr. Han-Way Huang for his admission and guidance. I would like to thank Dr. Nannan He, Dr. Puteri S. Megat Hamari, Dr. Xuanhui Wu, and Dr. Qiang Ye. Thank you for sharing the knowledge and assistance. It has been a precious and meaningful learning experience in Minnesota State University, Mankato. Financial support from the Xcel Energy through a grant from the Renewable Development Fund is gratefully acknowledged.

Last but not least, I would like to give my deepest gratitude to my grandmother Shimei Pan, mother Hongyu Zhao, my aunt Xinghua Zhao, my uncle Jian Tang, my uncle Guofeng Zhao, my aunt Jin Wo, and my cousins Ashton and Emma. I would not have made it without their unconditional and selfless love, care and encouragement.

TABLE OF CONTENTS

Chapter 1 : Introduction.....	1
1.1 Background.....	1
1.2 Renewable Energy Conversion and Energy Storage Systems.....	2
1.2.1 Wind Energy Conversion System.....	2
1.2.2 PV System.....	4
1.2.3 Energy Storage Systems	5
1.3 Background of Renewable Energy Integration to the Microgrid.....	6
1.3.1 Microgrid with RESs and ESSs	6
1.3.2 One-Stage DC-AC Power Conversion System.....	7
1.3.3 Two-Stage DC-DC-AC Power Conversion System	8
1.4 Research Objectives.....	10
1.5 Outline of Thesis.....	11
Chapter 2 : A Review of Multiport Converters	12
2.1 The Types of DC-AC Inverter	13
2.1.1 Single Phase Inverter	13
2.1.2 Three Phase Inverter	15
2.2 Principle of Inverter Operation	16
2.3 Improvement for Inverter Output.....	17
2.4 Summary	19

Chapter 3 Modeling and Controller Design of Proposed Inverter	20
3.1 The Proposed DC-AC Inverter	21
3.2 Modeling of Proposed Inverter	23
3.3 Controller Design of Proposed Inverter	24
3.3.1 d-q frame reference	25
3.3.2 Controller design analysis in standalone mode.....	30
3.4 Simulation of the standalone inverter	32
Chapter 4 : Inverter in Grid-connected Mode.....	35
4.1 Controller Design of Grid-Connected Inverter	35
4.1.1 Inverter-level controller design in d-q frame	35
4.1.2 System-level controller design in grid-connected mode.....	38
4.2 Experimental Setup for grid-connected inverters	40
4.2.1 Setup with microprocessor board.....	41
4.2.2 Setup with sampling sensors	43
4.2.3 Sequence setup at grid-connected mode	47
4.3 Experimental results and analysis	49
4.3.1 Steady response in grid-connected mode.....	50
4.3.2 The transient responses with grid	50
4.3.3 Quality analysis of the inverters	53
Chapter 5 Conclusions and Recommendations for Future Works	55

5.1 Conclusions.....	55
5.2 Recommendations for future work	56
Appendix.....	57
References.....	63
List of Publications	67

Chapter 1 : Introduction

This chapter introduces the background for this thesis: There is a need for the development of multiport converters to integrate renewable energy sources (RESs) with different types and capacities, and energy storage systems (ESSs) to the power grid. Based on this motivation, this chapter discusses the research objectives and outline of this thesis.

1.1 Background

Electricity infrastructure is the foundation of every country all over the world. The traditional power systems are centralized and built far away from the costumers. The sources like coal are limited in supply and unfriendly to the environment. In addition, it may need a long time to restore if there are power outages caused by natural disasters such as floods and hurricanes. For example, Hurricane Sandy left million customers without power for serval days across 15 states in August 2003 [1]. The widespread power outages in the wake of Hurricane Sandy cast light on the weakness of a centralized electric power system. As the demand for electricity grows, the penetration of distributed generation (DG) is gradually increasing in developed countries worldwide [2]. Due to the merits of renewable energy, RESs, such as wind turbine generators (WTGs) and photovoltaic (PV) panels are widely used to generate electricity.

Microgrids are introduced into electric power systems for managing the widespread penetration of renewable energy and DGs in power distribution networks [2]-[3]. The microgrids concept assumes a cluster of loads and microsources operating as a single

controllable system that provides both power and heat to its local area. This concept provides a new paradigm for defining the operation of distributed generation [2]. Power electronic converters play an important role in integrating various RESs, such as PV and wind energy systems, and ESS, such as batteries, into a microgrid and managing the power flows among different sources and the microgrid [4].

1.2 Renewable Energy Conversion and Energy Storage Systems

The basic characteristics of renewable energy systems are sustainable and clean. But the renewable energy also has intermittence. Therefore, both WTGs and PV panels are used in some applications to complement with each other, e.g., the solar energy is available in the daytime when the wind speed is low and the strong winds often occur when it's cloudy, rainy or at night. The energy storage devices like batteries are also used with RESs in case neither solar nor wind energy is available.

1.2.1 Wind Energy Conversion System

Wind energy conversion systems (WECS) are designed to convert the energy of wind movement into mechanical power, which typically uses a WTG. The mechanical energy will be transferred into making electricity and in windmills this energy is used to do work such as pumping water, mill grains, or drive machinery. Fig 1.1 shows the configuration of a WECS. The WTG can be a permanent magnet synchronous generator (PMSG), doubly fed induction generator (DFIG), induction generator, synchronous generator, etc. Wind energy acquired from the wind turbine is sent to the generator. To

achieve maximum power from the wind energy, the rotation speed of the generator is controlled by a pulse width modulation (PWM) converter. The output power of the generator is supplied to the grid through a generator-side converter and a grid-side inverter[5].

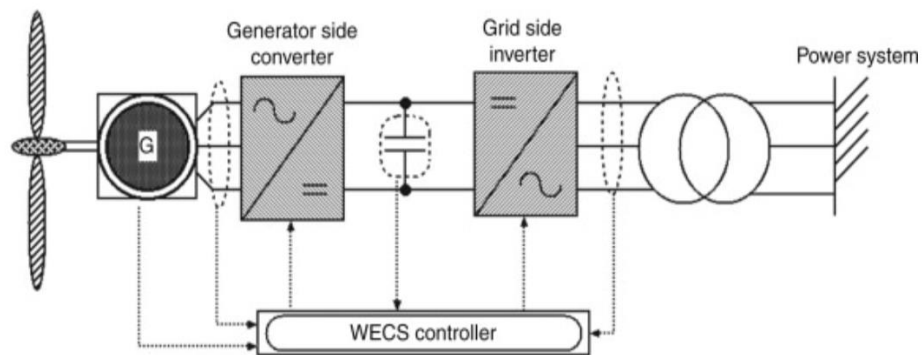


Fig 1.1 Configuration of WECS.

The mechanical power captured by the wind turbine can be formulated as:

$$P_t = \frac{1}{2} \cdot C_p(\lambda, \beta) \cdot \rho \cdot A \cdot v_w^3 \quad (1.1)$$

where ρ is the air density, A is the area swept by the blades, v_w is the wind speed, $C_p(\lambda, \beta)$ represents the power coefficient of the wind turbine, β is the wind turbine pitch angle, and λ is the tip-speed ratio (TSR), which is defined as

$$\lambda = \frac{\omega \cdot R}{v_w} \quad (1.2)$$

where ω and R represent the angular speed and the radius of the wind turbine, respectively. Since in the real application the wind speed may vary from time to time, the operating rotor

speed needs to be changed with the wind speed so that the maximum power can be generated by the WTG. Therefore, it is necessary to implement the maximum power point tracking (MPPT) algorithm to follow the MPP, which is changed with the wind speed.

1.2.2 PV System

A PV system is designed to supply usable solar power by means of PV. Fig 1.2 shows a typical PV system. The components mainly include PV panels and a power converter. The function of PV panels is to absorb and convert sunlight into electricity. Then, the power converter is to convert the time-variant voltage of the PV panels to a constant voltage required by the load or the grid. Meanwhile, the converter will regulate the PV panels to work in MPPT mode such that maximum power is generated.

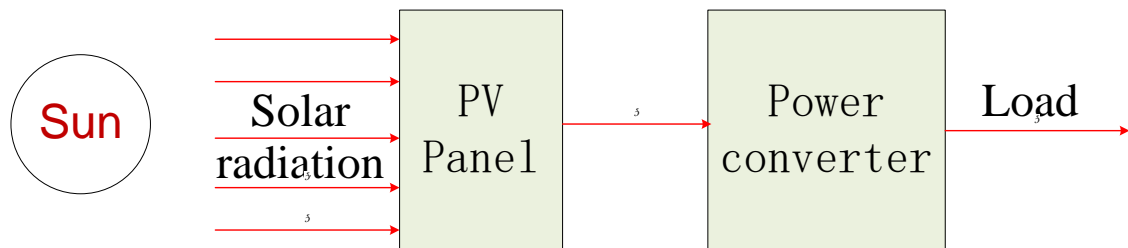


Fig 1.2 A typical PV system.

PV systems range from small, rooftop-mounted or building-integrated systems with capacities from a few to several tens of kilowatts, to large utility-scale power stations of hundreds of megawatts. Nowadays, most PV systems are grid-connected, while off-grid or stand-alone systems. The grid-connected systems are especially employed in residential or commercial area. A grid connected system is connected to a larger independent grid

(typically the public electricity grid) and feeds energy directly into the grid. In this thesis, the PV system will be connected with converters to regulate the output voltage and eject power into the grid.

1.2.3 Energy Storage Systems

RESs are alternative to fossil fuels due to the merits of cleanness and infinite. But the RESs like solar and wind energy are related to the weather conditions which cause the RESs will fluctuate independently. Therefore, the stochastic or intermittence characteristics should be taken into consideration. The ESSs are identified as a key solution to mitigate the intermittence of the RESs and provide an uninterruptible power supply (UPS) required by the load or grid [6].

While many forms of ESSs have been installed, pumped hydro storage systems are by far the most widely used, compressed air energy storage is the next largest, followed by batteries [7]. With the development of materials technology, batteries are now becoming a good candidate for the electrical energy storage system [8]. In this thesis, a battery is used as the energy storage device with RESs. Fig 1.3 shows a typical structure of an electrical energy system using a RES with a battery to supply a load.

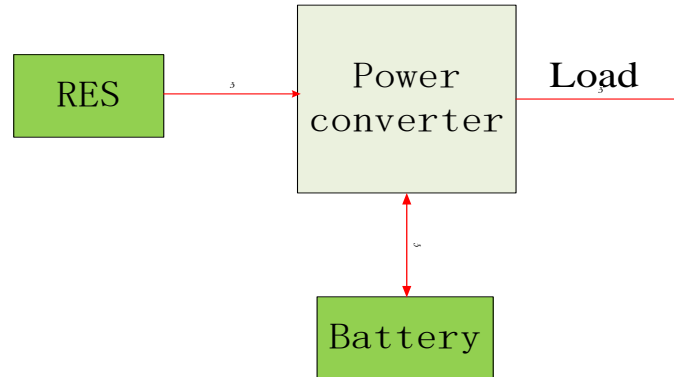


Fig 1.3 A typical power system with battery ESS

As shown in Fig 1.3, the power flow of the battery is bidirectional, this will ensure the whole system energy supply continuously and improve the reliability of the system. When the power generated by the RES is higher than the load, the battery is charged to store the surplus energy; when the RES power is not sufficient to supply the load, the battery will be discharged to provide the deficient power.

1.3 Background of Renewable Energy Integration to the Microgrid

1.3.1 Microgrid with RESs and ESSs

With the increasing demand of energy, microgrids are becoming a promising technology for integrating RESs [9]. Microgrids can operate at both grid-connected and stand-alone modes. There are two types of microgrids: AC and DC microgrids. AC microgrids are connected to the utility at the point of common coupling (PCC); DC microgrids can generate power from PV panels to some DC loads e.g. LED lighting [10]. But one of the biggest challenges of RESs is their uncertainty. This challenge will bring an

adverse effect on microgrid control and operation. To avoid and mitigate this disadvantage, there are several ways to solve the problem. One solution is to develop a RES prediction system which will provide information on how much renewable energy can be expected at a given point in time [11]. A good renewable energy prediction method will help achieve grid stability [11]-[15]. The other solution is to add EESs, such as batteries, in the microgrid. This is called hybrid microgrids by combining DC and AC systems. Nowadays, hybrid microgrids are growing rapidly and widely applied in power system, like residential areas.

According to the power conversion stage, there are two solutions to integrate RESs of different types and capacities to a microgrid: a one-stage DC-AC system and a two-stage DC-DC-AC system.

1.3.2 One-Stage DC-AC Power Conversion System

Fig 1.4 shows the configuration of this system, Due to this one stage of power conversion, this solution has high efficiency. However, in this solution, the double-line-frequency issue is inherited [16]. In one-stage DC-AC power conversion system, each source is directly connected to a DC-AC inverter. And then, the DC power from the renewable source will be converted to the AC required by the microgrid.

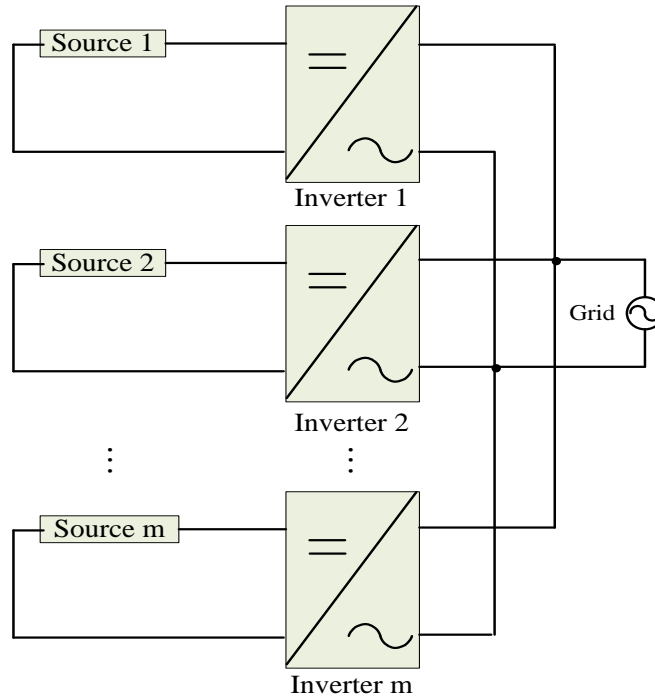


Fig 1.4 One-Stage DC-AC conversion system.

1.3.3 Two-Stage DC-DC-AC Power Conversion System

In a two-stage DC-DC-AC power conversion system, it consists of DC-DC converters and DC-AC inverters. First stage is a DC-DC converter which is used to step up the low time-variant voltage of each source to the high constant voltage. Second stage is DC-AC inverter to regulate the DC link voltage to AC for grid. There are two ways of this system.

Fig 1.5 shows the traditional way that each source will connect to one DC-DC converter. Another way is using a multiport DC-DC converter to interface all the sources. Fig 1.6 shows the multiport two-stage system. Compared to the traditional one, a multiport DC-DC converter has lower cost and higher power density. In this thesis, multiport DC-

DC converters of different topologies are developed for the DC-DC-AC power conversion system.

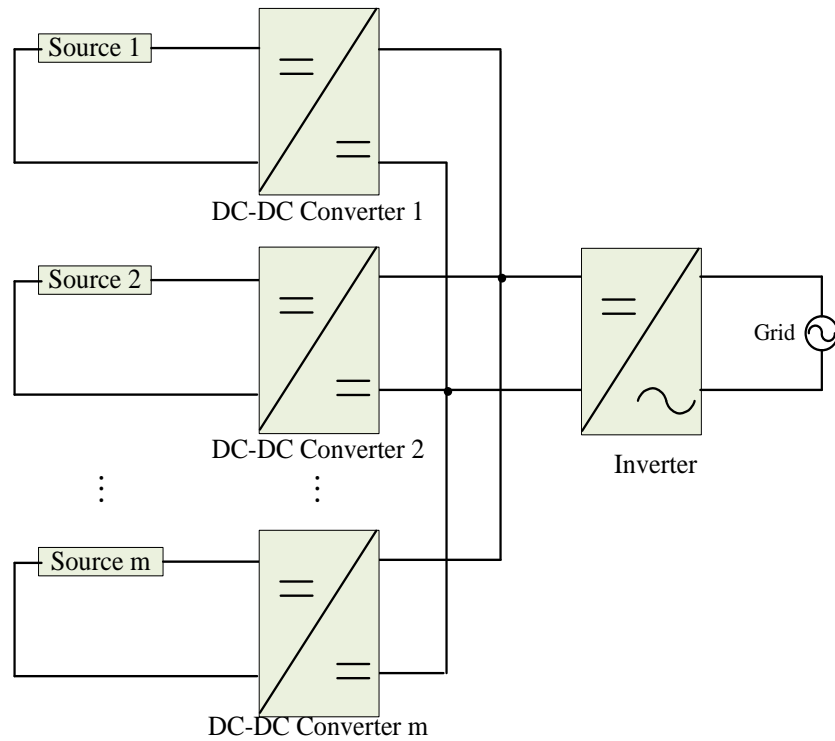


Fig 1.5 Traditional two-stage DC-AC system

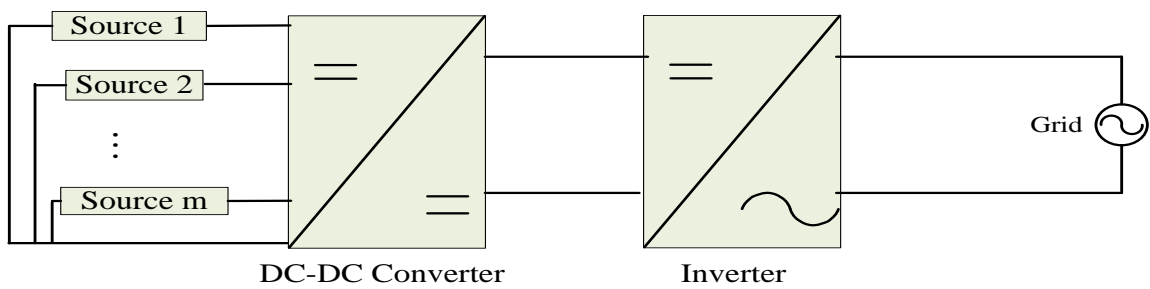


Fig 1.6 Multiport two-stage DC-AC system

1.4 Research Objectives

The objective of the research is to develop a multiport power converter for renewable energy conversion and integration. The objectives of this research are listed as follows:

Control in the d-q rotation frame: In real time applications, voltages and currents are sensed in stationary frame which are changed from time to time. Using d-q rotation frame will make computations and controllers design easy since the time-varying signals in the stationary frame will become constant values in the rotation frame. In this research, the PI controllers in d-q will be designed to make inverter works in both standalone and grid-connected modes.

Standalone mode: When the inverters work without the utility grid, it is called the standalone mode. The inverter remains as a basic source and generates sufficient power for the load.

Grid-connected mode: When the inverters are connected with the grid, the system can deliver power to the grid which is called the grid-connected mode. The inverter can match the voltage and frequency of grid accurately. In this thesis, the inverter can distribute the power equally by using droop control.

1.5 Outline of Thesis

This thesis will be organized as follows.

Chapter 2 reviews the typical topology using multiport converters to interface with hybrid wind and solar energy systems in residential power systems. The principle operation of inverter is also discussed.

Chapter 3 proposes a standalone multiport DC-AC inverter for wind/solar hybrid energy systems. The controllers design and simulation analysis are presented. Then the controllers designed in the d-q rotation frame is discussed. Finally, a prototype of the designed inverter is constructed and validated by results.

Chapter 4 introduces a single-phase grid-connected inductor-capacitor-inductor (LCL)-resonant circuit to achieve power distribution based on the multiport DC-AC inverter proposed in Chapter 3. Compared to the Chapter 3, this chapter will focus on power sharing, synchronization, droop control, and transient response. The quality of experimental results is discussed by analyzing its spectrum, e.g., total harmonic distortion (THD).

Finally, the thesis ends with conclusions, a summary of contributions, and recommendations for future work in Chapter 5.

Chapter 2 : A Review of Multiport Converters

Nowadays, the commonly used RESs are wind energy and solar energy. The most promising device in ESSs is battery which will also be applied. The multiport converters which share some components have lower cost and higher efficiency than conventional ones. Therefore, in many applications, converters at least have three ports to integrate different types of energy sources to a power grid. The first stage multiport DC-DC converters can step up the low, time-variant voltage to high, constant voltage required by the AC side. The second stage is a grid-connected DC-AC inverter which can regulate the voltage from DC to AC.

The multiport DC-DC converter topologies can be classified into two categories: nonisolated and isolated [17]. Nonisolated converters include various boost-type converters [18]-[22]. Their voltage ratios can be further increased by using the cascaded or coupled-inductor technique [22]-[24]. When the voltage regulation ratios are high, the isolated converters are preferable than nonisolated converters by properly designing the transformer's turn ratio. In addition, the isolated converters provide isolation between the input and output which is good for the safety [4].

The main types of DC-AC inverters include single-phase and three-phase. Normally, three-phase systems are used when the electrical power is distributed to the industry or commercial buildings. Single-phase systems are used primarily in low voltage such as residential [25].

This chapter reviews different types and the principle operations of DC-AC inverters.

2.1 The Types of DC-AC Inverter

An inverter is an electrical device that converts the DC power into the AC power. There are many ways to classify DC-AC inverters. One way is based on the nature of DC source feeding the inverter. It has voltage source inverter (VSI) and current source inverter (CSI). VSI has a constant voltage at its output terminals and the output voltage does not depend on the load, the output current is determined by the load. In this thesis, the inverter mentioned later belongs to the VSI. For VSI, it contains single phase inverter and three phase inverter.

2.1.1 Single Phase Inverter

The single-phase inverter mainly has two topologies: one is half bridge inverter, the other is full bridge inverter. The basic building block is the inverter leg. Fig. 2.1 shows the structure of half bridge inverter. The half bridge inverter has two switches in one leg. S_1 and S_2 are switched using frequency modulation in a complementary manner. When S_1 is on, the energy is supplied from the source to the load. The positive current flows to the load. And the output voltage is $+V_{dc} \cdot d_1$, where d_1 is the duty cycle of the S_1 . When S_2 is on, it's a negative current flow. The output voltage is equal to $-V_{dc} \cdot d_2$. In half bridge, the time for S_1 on is kept for half a period and 0 for the following period. So the output voltage is half of the input voltage.

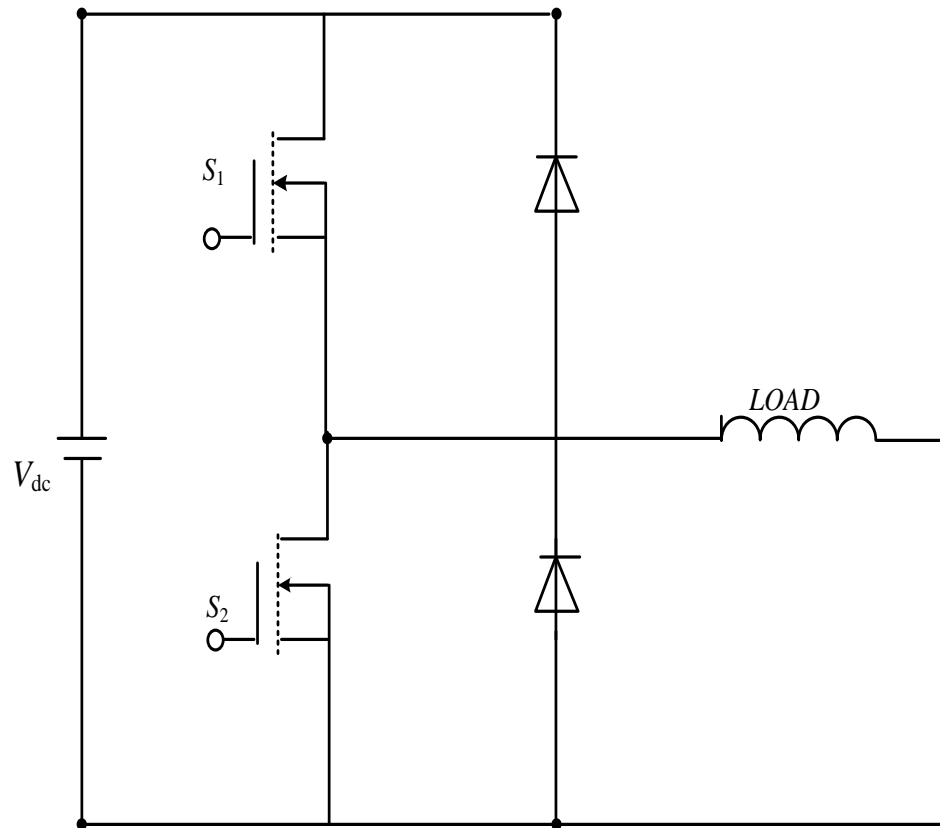


Fig. 2.1 Half bridge inverter topology

Fig. 2.2 shows the full bridge inverter topology. Two inverter legs are connected in parallel and four switches are used. The switches in one leg are complementary. When the switch S_1 , S_4 are on, S_2 and S_3 off, the output voltage is equal to V_{dc} . Instead, the output voltage is equal to $-V_{dc}$. Based on the half bridge, $V_A = d_A \cdot V_{dc}$ and $V_B = d_B \cdot V_{dc}$. Therefore, the output voltage of load is equal to $(d_A - d_B) \cdot V_{dc}$. For a sinusoidal output, $(d_A - d_B)$ must vary sinusoidally. So the magnitude and frequency can be controlled by controlling the duty cycle.

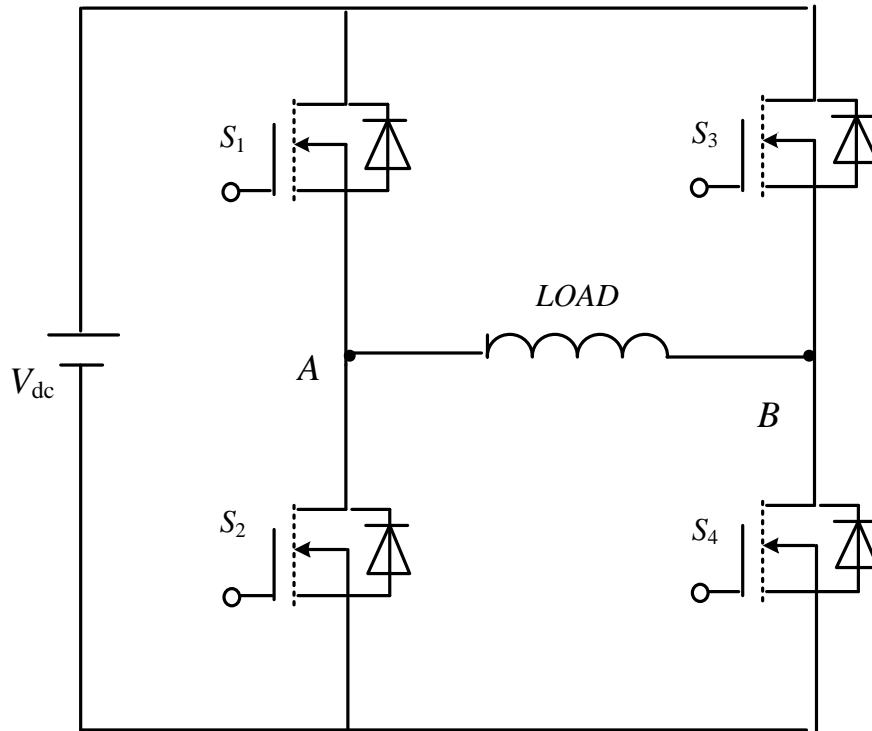


Fig. 2.2 Full bridge inverter topology

As discussed above, the main difference between the half bridge and full bridge is the maximum value of output voltage. The full bridge topology provides double the output voltage compared to the half bridge topology when the supply voltage is same. So, the full bridge is good for the high power requirement. In this thesis, full bridge topology is the fundamental to design the inverter.

2.1.2 Three Phase Inverter

Three phase inverters are used for variable-frequency drive applications and for high power applications such as HVDC power transmission. Fig. 2.3 shows a basic three-phase inverter consists of three single phase inverter switches each connected to one of the

three load terminals. Three phase VSI has 120 degree mode and 180 degree mode which depends on the conduction state of each electronic device. The voltage of each line has the same magnitude but with 120 degree shift.

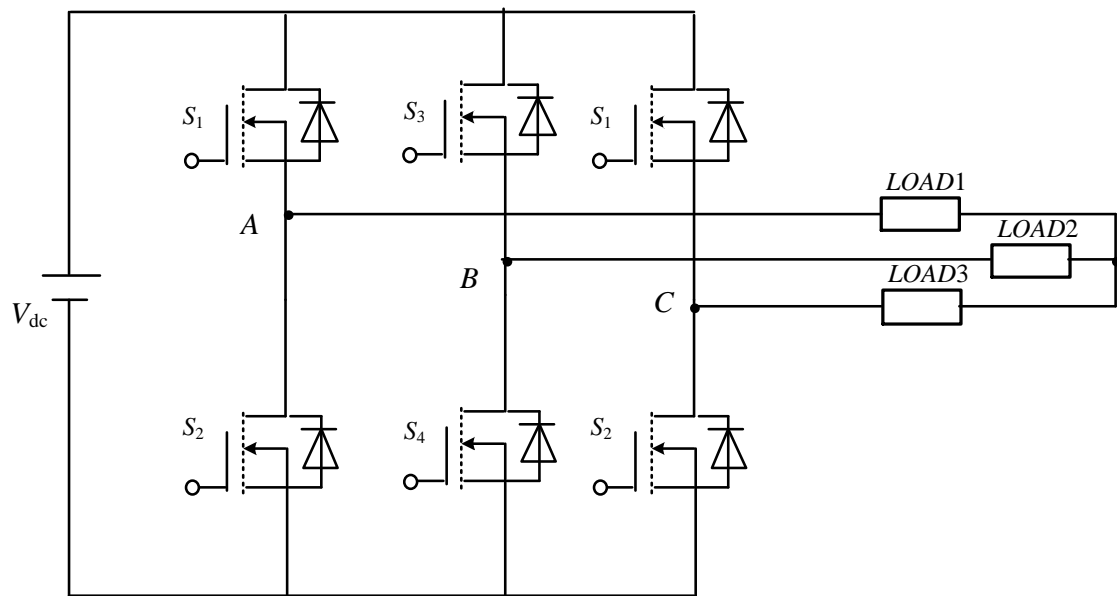


Fig. 2.3 Three phase inverter topology

2.2 Principle of Inverter Operation

As mentioned above, the key for inverters generating AC power is the modulation switching method. The pulse width modulation (PWM) method is a commonly used technique to reduce the average power delivered by an electrical signal, by effectively chopping it up into discrete parts. By controlling the pulse width, the frequency and amplitude of the inverter output voltage could be controlled. There are many different PWM techniques. The most commonly used modulation method is sinusoidal PWM (SPWM) which can get a desired sinusoidal voltage. Fig. 2.4 shows the SPWM for inverter.

As shown in Fig. 2.4 (a), the desired reference signal is compared with a triangular carrier wave, which results in the chopped square pulses. The frequency of the carrier wave is switching frequency. And the switching frequency is normally much higher than the modulating frequency. According to the averaging theory, as long as the switching frequency is high enough, the average of the pulses over one switching period would be able to well approximate the original signal [26]. Fig. 2.4 (b) and (c) show the switches of the same legs which are operated in a complementary way to avoid short circuit.

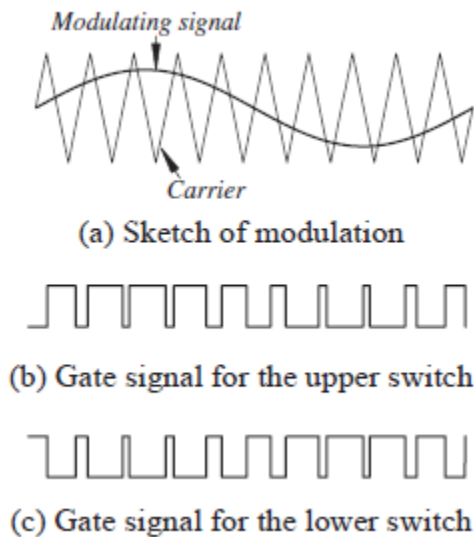


Fig. 2.4 SPWM for a single-phase inverter

2.3 Improvement for Inverter Output

Harmonic components that degrade the power quality inevitably exist in the inverter output voltage because of the PWM method. Harmonics are voltages or currents that operate at a frequency that is an integer (whole-number) multiple of the fundamental

frequency, which may distort its wave shape. So, the total harmonic distortion (THD) is a measurement of all harmonic components to the power of the fundamental frequency. The lower THD means the better quality.

A filter is often installed between the inverter and the load or grid to improve the quality[27]. There are some various filters including passive power filter (PPF), active power filter (APF) and hybrid filter APF (HAPF). Fig. 2.5 shows the most commonly used passive inverter filters, LC filters and LCL filters.

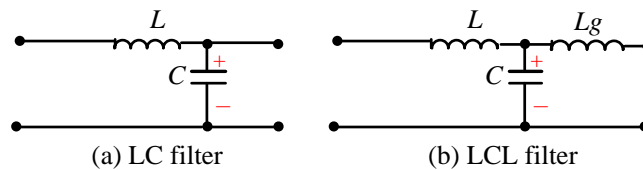


Fig. 2.5 The circuit model of the passive power filters

The cut-off frequency f_c of the LC filter is

$$f_c = \frac{1}{2 \cdot \pi \cdot \sqrt{L \cdot C}} \quad (2.1)$$

thus, it can filter out the harmonics located at frequencies higher than f_c . But it may cause a resonance which would magnify the harmonic current components at f_c and leads to the voltage THD higher. Meanwhile, the f_c should be much lower than the switching frequency f_{sw} to filter out the switching harmonics. And it has to be high enough to provide bandwidth for the controllers. It's usually chosen as:

$$\frac{f_{sw}}{3} \leq f_c \leq \frac{f_{sw}}{2} \quad (2.2)$$

The output impedance of inverter plays an important role in power sharing [28]. The types of the line impedances contain resistive, resistive-inductive and others. Since most output filters inductor, the output impedance of inverter is usually inductive.

2.4 Summary

From the literature review described above, the principle operation for inverters is PWM method. To get higher quality of output waveform, the filter is necessary. In this work, the full-bridge DC-AC inverter is implemented with SPWM method which can generate AC power. And the output filter will be chosen differently in both standalone and grid-connected mode.

Chapter 3 Modeling and Controller Design of Proposed Inverter

Single-phase PV inverters have been widely installed in residential power systems to meet full or partial load demand. This work employs a typical topology with two-stage four-port converters. As shown in Fig. 3.1, the multiport converters consist of a boost DC-DC converter which interfaces with three ports, wind turbine, PV panel and batteries in first stage and a DC-AC inverter in second stage. The function of the boost converter is voltage amplification and maximum power point tracking (MPPT). After stepping up the time-variant, low-level source voltages to a constant high-level voltage which is required by the cascaded DC-AC inverter, the inverter can generate sinusoidal waveform then eject to the load or grid. The proposed DC-AC inverter is based on full-bridge with capacitor and inductors.

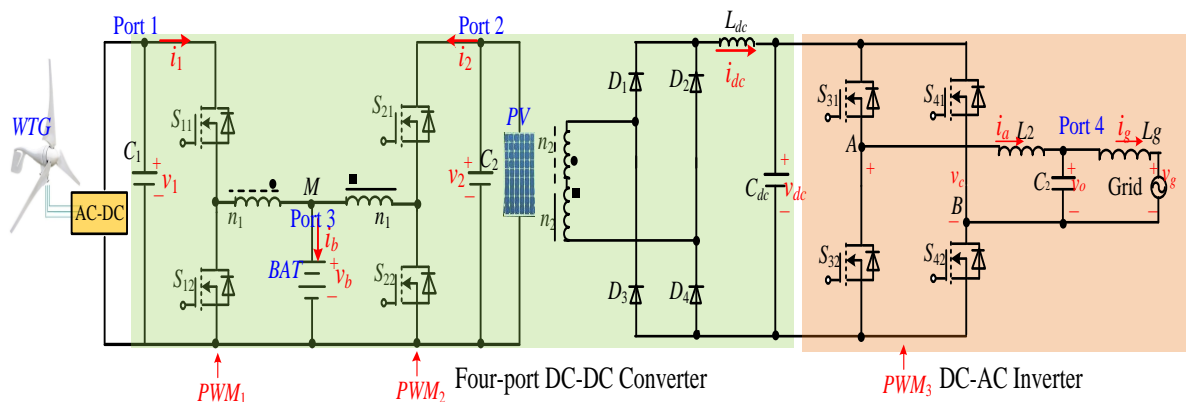


Fig. 3.1 Topology

3.1 The Proposed DC-AC Inverter

The proposed inverter designed in this work is single-phase based on full bridge with controllable switches and output filters. The full bridge is also known as H-bridge. It consists of four controllable switches like metal-oxide-semiconductor field effect transistor (MOSFET) or GaN board, capacitors and inductors.

To avoid creating a short circuit of the DC source, the signals are generated in each leg of the bridge reversely. The bottom gate control is the inverse of the top, but the same to the top of the parallel leg. That means the signals of S_{31} and S_{32} in Fig. 3.1 are in complementary manner, but S_{32} and S_{41} are correspondingly same. But S_{31} and S_{32} are never closed at same time, otherwise it would cause a short circuit from v_{dc} to the ground. To avoid this shoot-through, a deadtime is implemented in real switches. If the deadtime is too long and the voltage loop decreases, it will cause the voltage loss and crossing zero distortion. In this work, 0.2 microseconds deadtime is selected.

The gates of the H-bridge are driven by a PWM generator. The switching frequency f_{sw} of PWM signals is usually chosen as high as possible to reduce current ripple in the inductor. In this work, the period time of switching, i.e., T , is 10 microseconds. When the switches are on and off, the proportion of “ON” time to the period time is defined as duty cycle (d). If d_3 is defined as the ON time of S_{31} , then $v_A = v_{dc} \cdot d_3$, $v_B = -v_{dc} \cdot (1-d_3)$. Therefore, the control voltage $v_c = v_{dc} \cdot (2d_3-1)$. Fig. 3.2 shows the drive waveform for four switches. To control the output voltage of inverter, we can control the duty cycle.

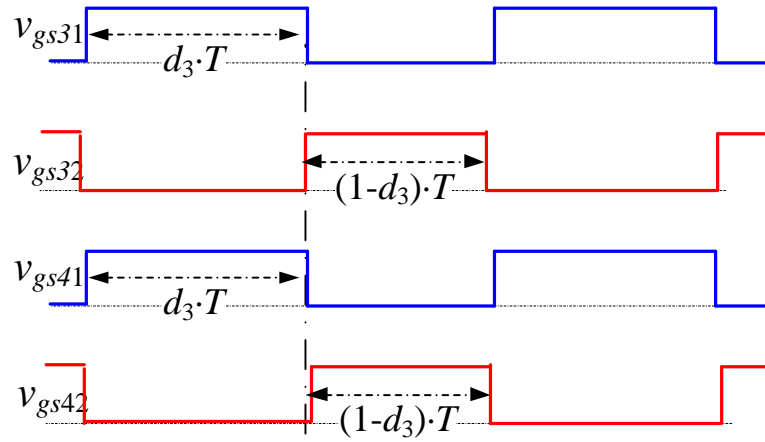


Fig. 3.2 Drive waveform for switches

Fig. 3.3 shows the experimental waveforms of the drive signals which are down sampling. This tests that the driver of proposed inverter is working.

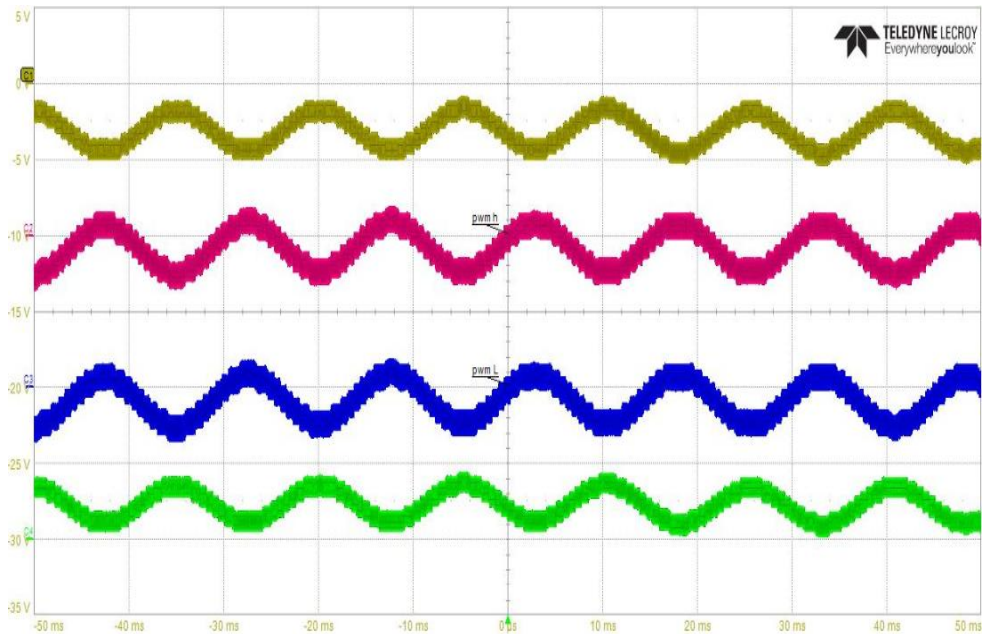


Fig. 3.3 Experimental waveforms for drive signals for 100 microseconds

Since the inverter requires an output filter to limit the high frequency current ripple [29], the LCL output filter is selected at grid-connected mode. For the standalone mode, the inverter will connect with the resistive loads. Fig. 3.4 shows the simplified circuits at two modes. Once one single-phase DC-AC inverter working well, parallel connected inverters can simulate the grid system. The inverters need to detect the voltage and frequency from the grid, then generate different output with power need. One inverter can be simulated as the source because of its the stable output at standalone mode.

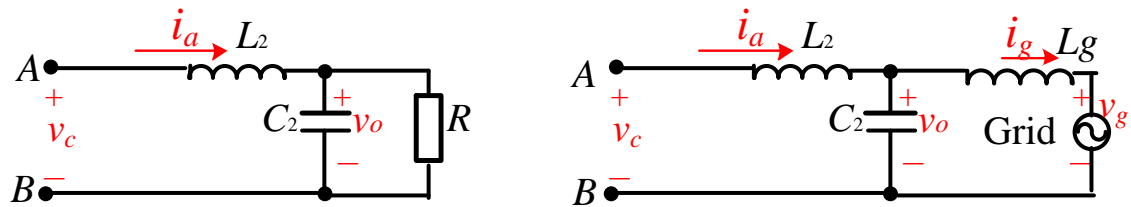


Fig. 3.4 Simplified inverter circuits at standalone and grid-connected mode

3.2 Modeling of Proposed Inverter

The main part of the whole work is modeling and designing the control method. How to design the controller is the key to the power electronics systems. Before designing the controller, the converter needs to be modelled. The most popular way of modeling is to use state space averaging method (SSAM) which is based on the small-signal model of the whole system. By using a formal method for deriving the small-signal AC equations of a switching converter, the differential equations in the different operation stages can be expressed. In addition, there are some computer programs existing which utilize the SSAM, for example, Matlab Simulink.

As shown in Fig. 3.4, the state-space models of inverter connecting with load R can be found as follows:

$$\begin{cases} v_c = v_o + L_2 \cdot \frac{di_a}{dt} + r \cdot i_a \\ i_a = C_2 \cdot \frac{dv_o}{dt} + \frac{v_o}{R} \end{cases} \quad (3.1)$$

where v_c is the control voltage of the H-bridge between nodes A and B; i_a is the current flowing through the inductor of L_2 ; v_o is the voltage of the inverter; r is the resistance of L_2 . Then the small-signal model with $\dot{x} = A \cdot x + B \cdot u$ form can be expressed as follows:

$$\dot{x} = \underbrace{\begin{bmatrix} \frac{-r}{L_2} & \frac{-1}{L_2} \\ \frac{1}{C_2} & \frac{-1}{R \cdot C_2} \end{bmatrix}}_A \cdot x + \underbrace{\begin{bmatrix} \frac{V_{dc}}{L_2} \\ 0 \end{bmatrix}}_B \cdot u \quad (3.2)$$

where $x = [i_a, v_o]^T$ and $u = d_3$.

3.3 Controller Design of Proposed Inverter

Every switching power converter consists of a switching network and some sort of input and output filters. By controlling the switching network, processing power with high efficiency and reliability is achieved in a desired and controlled manner. AC or DC power presented at the input of the switching network is transformed into either AC or DC output power and delivered to some load based on the nature of the converter. The task of controlling switches become evidently important, when processing an input power for

certain desired output power. A controller is a subsystem or a process assembled for the purpose of controlling the output of a plant such as a switching mode converter.

For the proposed inverter, the controllers can be designed based on the simplified model as shown in Equation (3.2), the transfer function of $v_o(s)/i_a(s)$ and $i_a(s)/d_3(s)$ can be derived as follows:

$$g_{cv}(s) = \frac{v_o(s)}{i_a(s)} = \frac{R}{R \cdot C_2 \cdot s + 1} \quad (3.3)$$

$$g_{ci}(s) = \frac{i_a(s)}{d_3(s)} = \frac{1}{L_2 \cdot s + r} \quad (3.4)$$

Fig. 3.5 shows the signals flows of the PI controller and the plant of the standalone inverter. The controllers include the voltage controller $G_{cv}(s)$ and current controller $G_{ci}(s)$, which are designed to control the inverter voltage and current, respectively.

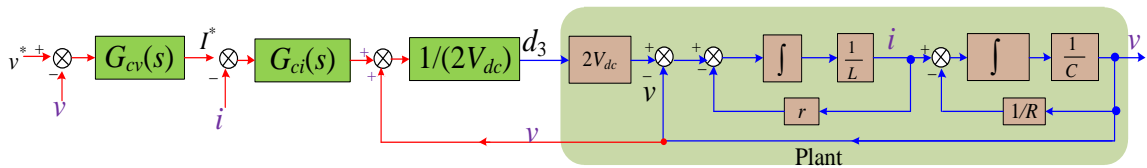


Fig. 3.5 Signal flows of the PI controller and the plant

3.3.1 d-q frame reference

The inverter generates AC signals which means the values of voltage and current are time-variant. But it will be easier to regulate signals as constant values by using PI controller. To make computations more easily, the d-q transformation which converts the

time-variant values to constant is used. It's a form of transformation between stationary and rotating frames. It is much easier to perform analysis and design controllers for three phase converters in DQ rotating frame because all time-varying state variables of the converter become DC time-invariant, hence only one operating point needs to be defined and considered for analysis.

For single phase inverter, the imaginary orthogonal circuit concept is introduced to create the additional orthogonal phase information [30]. The imaginary orthogonal circuit has the same circuit components and parameters as the real circuit. However, the imaginary circuit has 90 degrees phase shifted with respect to the phase in the real circuit. There are two ways to create the phase shifted. One is to differentiate output voltage and inductor current of the real circuit, a 90-degree phase shifted output voltage and inductor current can be created for the imaginary circuit [27]. Alternative way is to delay the real circuit variables for quarter period.

Fig. 3.6 shows the vector I can be decomposed into two components I_α and I_β in the stationary α - β frame. The current signal I can be transformed to the d-q frame using the time delay method. The actual current signal can be referred as the real current on d axis and the time delayed signal as the imaginary current on q axis, where corresponds to the α and β respectively. And the rotating frame d-q has the same angular frequency with the fundamental frequency of inverter. A rotating vector in the α - β frame becomes a constant vector in d-q frame due to the rotation of the reference plane itself. Therefore, the

components I_α and I_β change phase angle and magnitude of the vector I , while the I_d and I_q are constant at any time and only depend on the magnitude of vector I not its position.

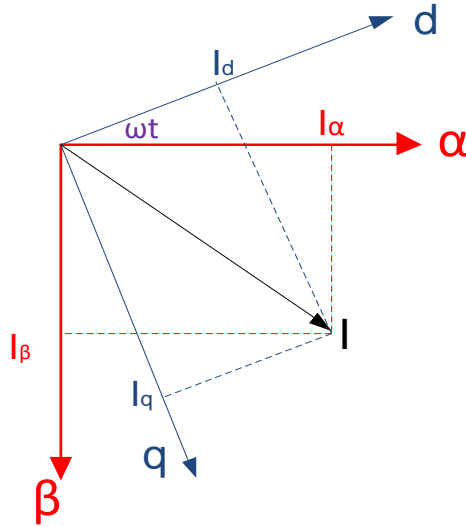


Fig. 3.6 d-q transformation

According to the characteristic of d-q frame, the transformation matrices are non-singular and orthogonal. Therefore $T^T = T^{-1}$ and $T \cdot T^{-1} = I$. The equations that describe the relationship between α - β and d-q frame are given as follows:

$$\begin{bmatrix} x^{(d)} \\ x^{(q)} \end{bmatrix} = \underbrace{\begin{bmatrix} \sin \omega t & -\cos \omega t \\ \cos \omega t & \sin \omega t \end{bmatrix}}_T \cdot \begin{bmatrix} x^{(\alpha)} \\ x^{(\beta)} \end{bmatrix} \quad (3.5)$$

$$\begin{bmatrix} x^{(\alpha)} \\ x^{(\beta)} \end{bmatrix} = \underbrace{\begin{bmatrix} \sin \omega t & \cos \omega t \\ -\cos \omega t & \sin \omega t \end{bmatrix}}_{T^{-1}} \cdot \begin{bmatrix} x^{(d)} \\ x^{(q)} \end{bmatrix} \quad (3.6)$$

As shown in Fig. 3.7, build a simulation with a AC input $v_o = 10 \cdot \sin(2\pi \cdot t)$. The block to get dq transformation is based on the matrices T . Then delay the input for a quarter of period to create the orthogonal axis. The v_b is delayed a quarter of sample time compared to v_a . To get the same angle, the phase locked loop (PLL) block is used too.

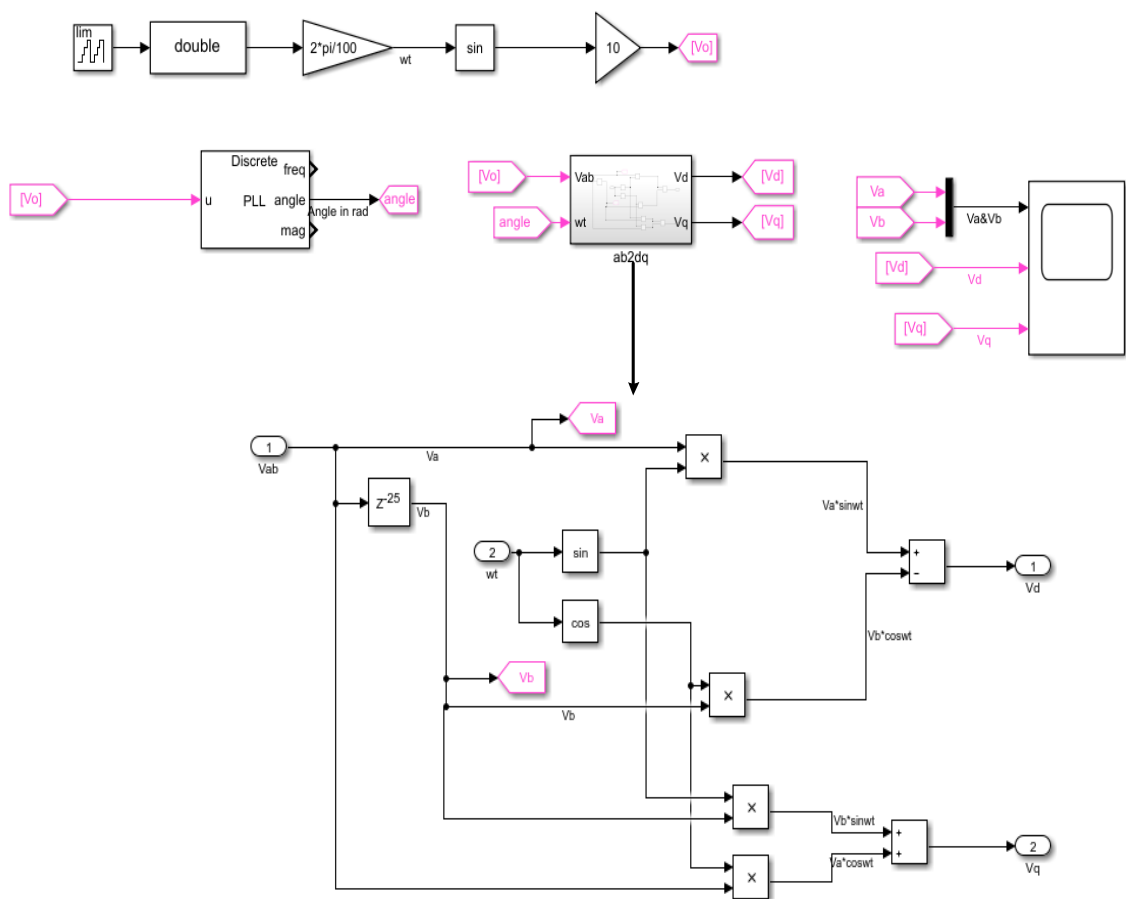


Fig. 3.7 Simulation to test dq frame

As shown in Fig. 3.8, the time delayed method works to create an imaginary orthogonal circuit. It takes around 0.05s to get the stable values in d-q frame. During the steady state, the value of voltage in d axis is 10 which is equal to the magnitude of input

voltage. And the value in q axis is 0. Therefore, the transformation matrices to converter signal into the d-q frame is correct.

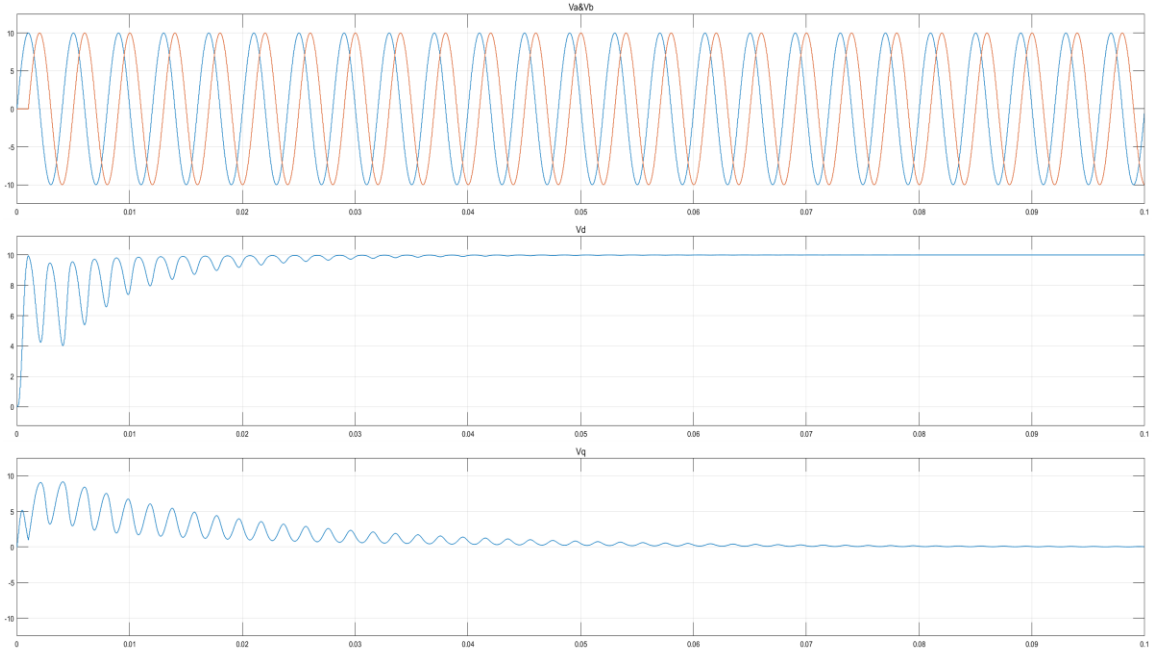


Fig. 3.8 Simulation waveforms of dq transformation

The differential equations of standalone inverter in d-q frame can be derived as follows:

$$L_2 \cdot \begin{bmatrix} \frac{di_{ad}}{dt} \\ \frac{di_{aq}}{dt} \end{bmatrix} = \begin{bmatrix} v_{cd} \\ v_{cq} \end{bmatrix} - \begin{bmatrix} v_{od} \\ v_{oq} \end{bmatrix} - r \cdot \begin{bmatrix} i_d \\ i_q \end{bmatrix} - \underbrace{\begin{bmatrix} 0 & -\omega \cdot L_2 \\ \omega \cdot L_2 & 0 \end{bmatrix}}_{K_1} \cdot \begin{bmatrix} i_d \\ i_q \end{bmatrix} \quad (3.7)$$

$$C_2 \cdot \begin{bmatrix} \frac{dv_{ad}}{dt} \\ \frac{dv_{aq}}{dt} \end{bmatrix} = \begin{bmatrix} i_{ad} \\ i_{aq} \end{bmatrix} - \frac{1}{R} \begin{bmatrix} v_{od} \\ v_{oq} \end{bmatrix} - \underbrace{\begin{bmatrix} 0 & -\omega \cdot C_2 \\ \omega \cdot C_2 & 0 \end{bmatrix}}_{K_2} \cdot \begin{bmatrix} v_{od} \\ v_{oq} \end{bmatrix} \quad (3.8)$$

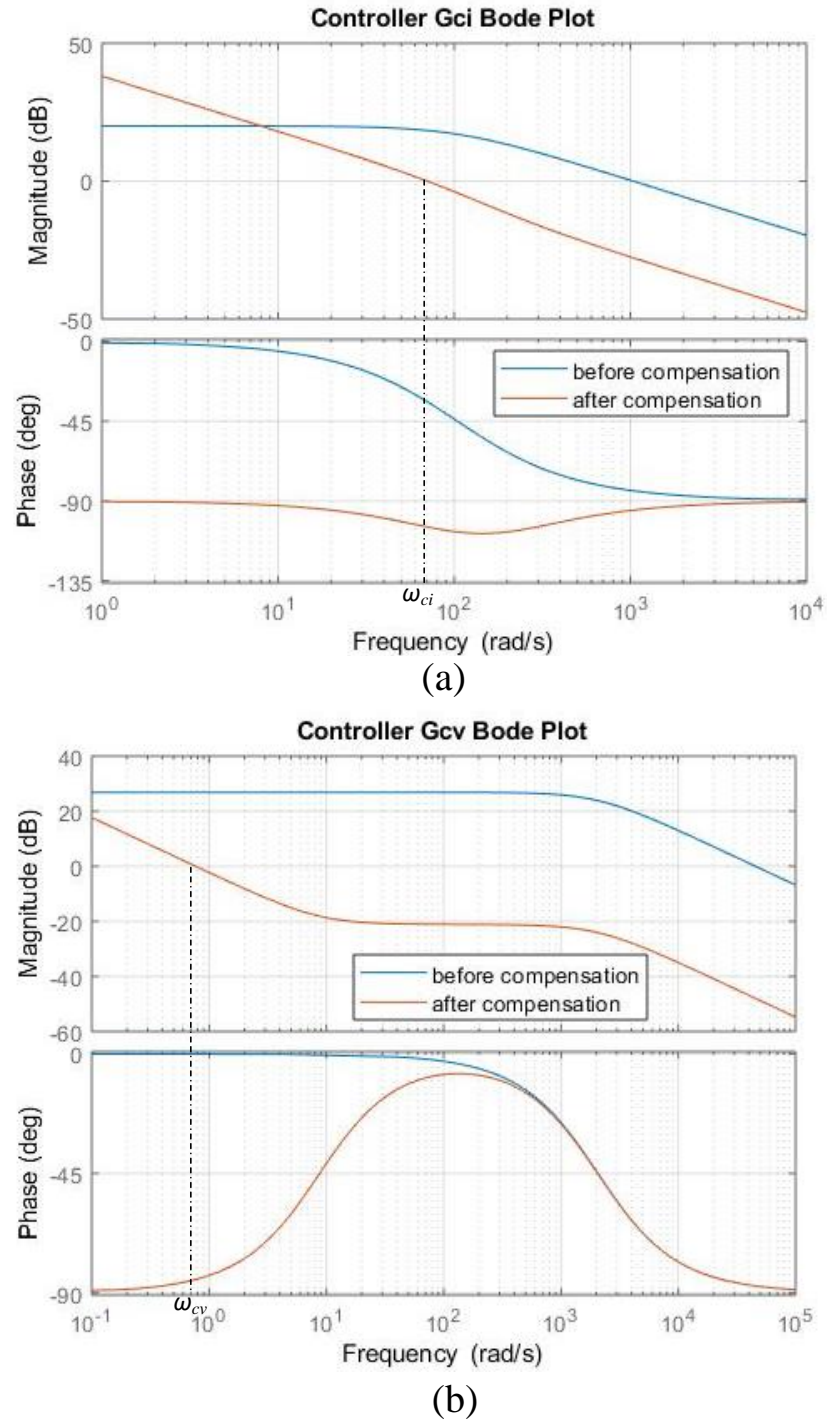


Fig. 3.10 Bode plots of inverters before and after using controllers

3.4 Simulation of the standalone inverter

Based on the modeling and controller designing, it's easy to build a simulation of the standalone inverter in Matlab Simulink. As shown in Fig. 3.11, the PV array block can simulate the PV panel. The parameters of capacitor and load can be set as real. In the U.S., the standard combination for voltage and frequency is 110 V (RMS value) and 60 Hz. Since the control of duty cycle, the reference value of DC link voltage is chosen as 190 V.

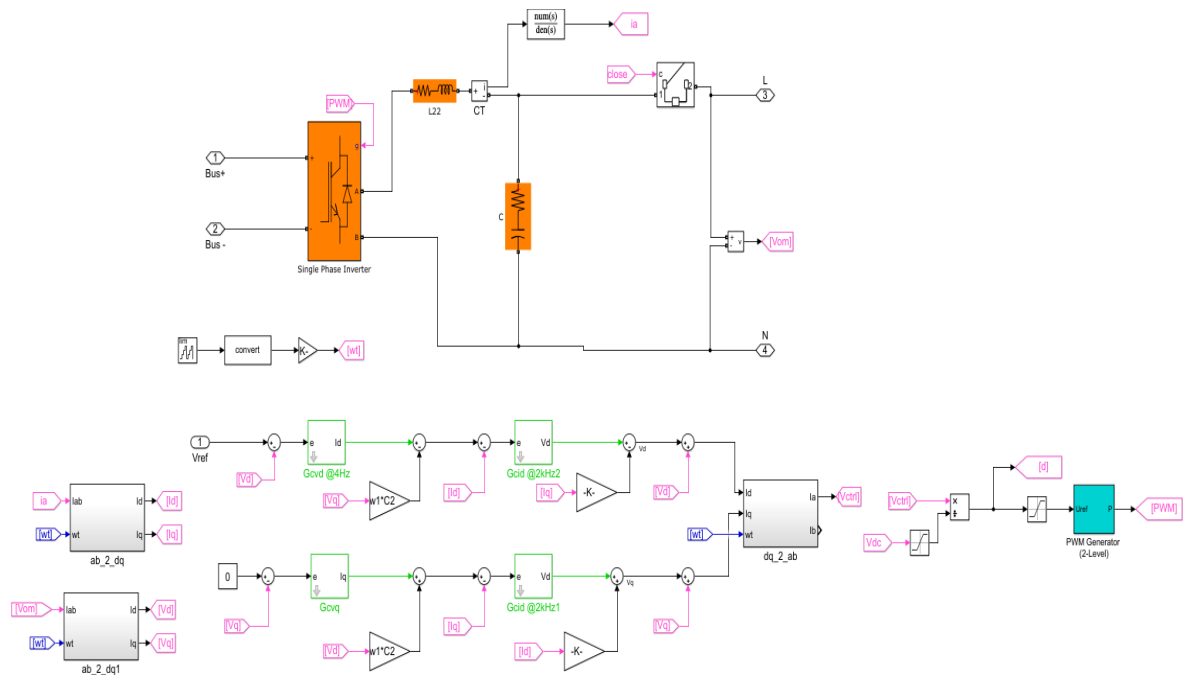


Fig. 3.11 Simulation of standalone inverter

The power can be defined by setting the numbers of parallel strings and series-connected modules of per string. The input of sun irradiance and cell temperature can simulate the situation in real life. Fig. 3.12 shows the I-V and P-V characteristics at 1000

W/m^2 and 25°C . The maximum power can up to 700 W at 230 V. The maximum short-circuit current is around 3.5 A. The maximum open-circuit voltage is up to 280 V.

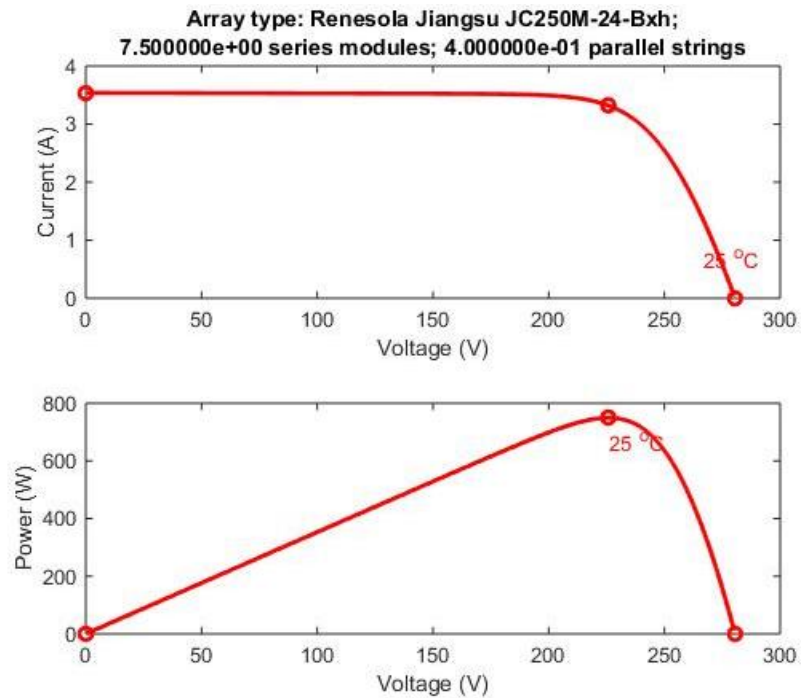


Fig. 3.12 I-V and P-V characteristics

Fig. 3.13 shows the single flows of inverter in the simulation. The current through the inductor and the voltage of the inverter can be measured by the measurement blocks. The block to do d-q transformation has been verified in Fig. 3.8. Therefore, the signals can be calculated in the d-q frame and also feedback to the controllers. The PI controllers can regulate the current and voltage.

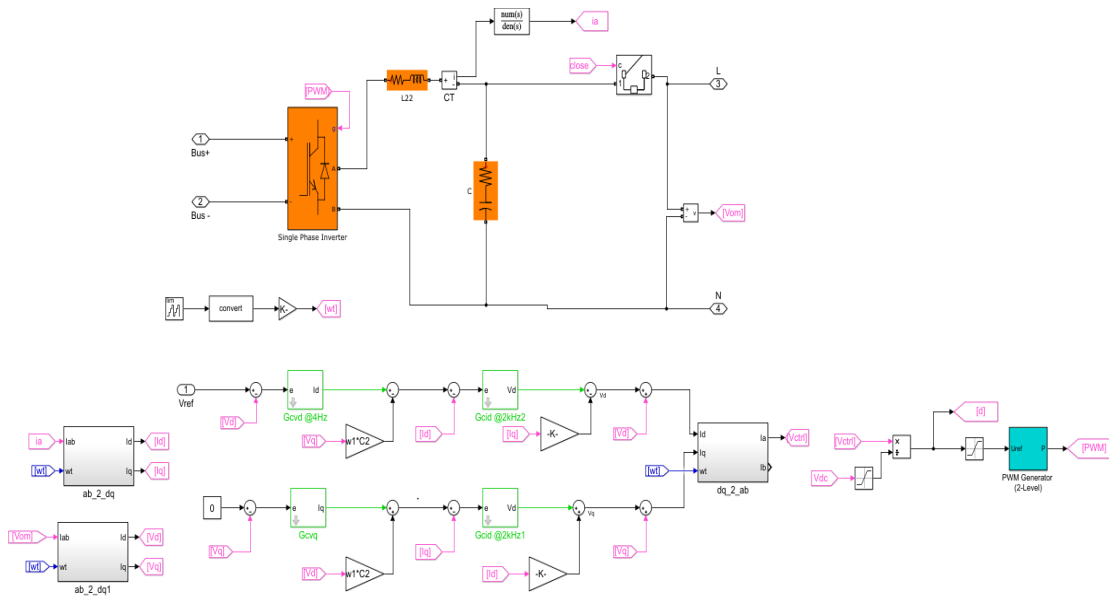


Fig. 3.13 Simulation design of the standalone inverter

Fig. 3.14 shows the simulation result. The voltage of inverter and current through the inductor are both stable. The total harmonic distortion (THD) of voltage is less than 0.5% which testified the effectiveness of inverter's controllers.

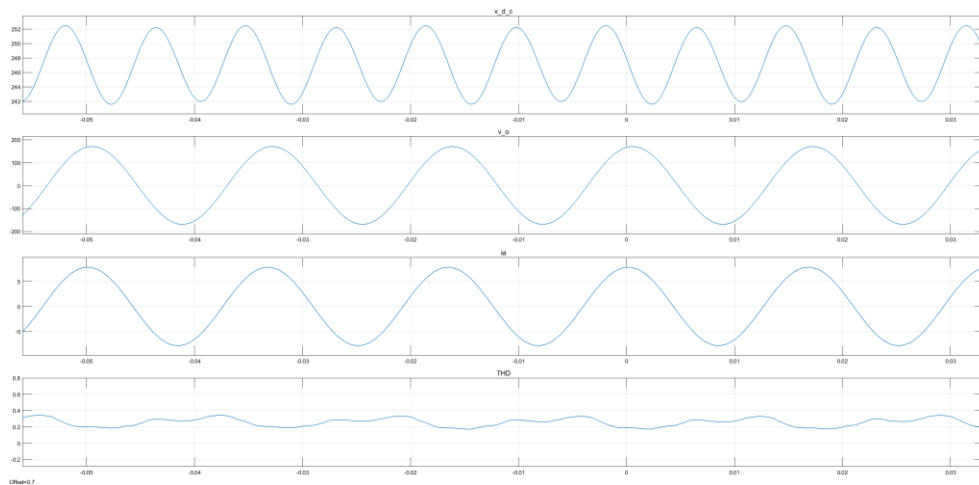


Fig. 3.14 Simulation results when inverter works in the standalone mode.

Chapter 4 : Inverter in Grid-connected Mode

As discussed in Chapter 3, the proposed inverter can work stably in standalone mode. To integrate different energy sources to the utility grid, it's required that the inverters can also work in grid-connected mode. This chapter will discuss how to design grid-connected inverters including the modeling and controller design. The setup and analysis of experiment results are also presented.

4.1 Controller Design of Grid-Connected Inverter

When the inverters connect to the grid, it needs synchronize the voltage with the grid. The first step is to use the phase lock loop (PLL) algorithm. The PLL block can test the voltage and frequency with the grid. Once the inverters can get the signals in phase, the inverter-level controller will be developed to regulate the grid current with sinusoidal waveform. Then, the system-level droop control will be used to achieve the power sharing among inverters in the microgrid.

4.1.1 Inverter-level controller design in d-q frame

As shown in Fig. 3.4, when the inverters connect to the grid, the state-space models of inverter can be found as follows:

$$\begin{cases} v_c = v_o + L_2 \cdot \frac{di_a}{dt} + r \cdot i_a \\ v_o = L_g \cdot \frac{di_g}{dt} + r \cdot i_g + v_g \\ i_a = C_2 \cdot \frac{dv_o}{dt} + i_g \end{cases} \quad (4.1)$$

where v_c is the output voltage of the H-bridge between nodes A and B; i_a is the current flowing through the inductor of L_2 ; v_o and v_g are the voltage of the inverter and the grid, respectively; r is the resistance of L_2 and L_g . It can be simplified as follows:

$$\begin{cases} v_c = L_g \cdot \frac{di_g}{dt} + r \cdot i_g + V_g + L_2 \cdot \frac{di_a}{dt} + r \cdot i_a \\ \frac{dv_o}{dt} = \frac{d\left(L_g \cdot \frac{di_g}{dt} + r \cdot i_g + V_g\right)}{dt} = L_g \cdot \frac{d^2i_g}{dt^2} + r \cdot \frac{di_g}{dt} + \frac{dV_g}{dt} \\ i_a = C_2 \cdot \frac{dv_o}{dt} + i_g = C_2 \cdot L_g \cdot \frac{d^2i_g}{dt^2} + C_2 \cdot r \cdot \frac{di_g}{dt} + C_2 \cdot \frac{dV_g}{dt} + i_g \\ \frac{di_a}{dt} = C_2 \cdot L_g \cdot \frac{d^3i_g}{dt^3} + C_2 \cdot r \cdot \frac{d^2i_g}{dt^2} + C_2 \cdot \frac{d^2V_g}{dt^2} + \frac{di_g}{dt} \end{cases} \quad (4.2)$$

Therefore the differential equation in the α - β stationary frame can be found as follows:

$$v_c^{(\alpha\beta)} = \underbrace{L_2 \cdot C_2 \cdot L_g}_{a_3} \cdot \frac{d^3i_g^{(\alpha\beta)}}{dt^3} + \underbrace{(L_2 + L_g) \cdot C_2 \cdot r}_{a_2} \cdot \frac{d^2i_g^{(\alpha\beta)}}{dt^2} + \underbrace{(L_g + L_2 + C_2 \cdot r^2)}_{a_1} \cdot \frac{di_g^{(\alpha\beta)}}{dt} + \underbrace{2 \cdot r \cdot i_g^{(\alpha\beta)}}_{a_0} \quad (4.3)$$

With the d-q transformation mentioned in Equation (3.5), the third differential of current can be transformed into d-q frame as follows:

$$\begin{aligned} \underbrace{L_2 \cdot C_2 \cdot L_g}_{a_3} \cdot \frac{d^3i_g^{(\alpha\beta)}}{dt^3} &= \underbrace{L_2 \cdot C_2 \cdot L_g}_{a_3} \cdot \frac{d^3\left(T^{-1} \cdot i_g^{(dq)}\right)}{dt^3} \\ &= v_c^{(\alpha\beta)} - \underbrace{(L_2 + L_g) \cdot C_2 \cdot r}_{a_2} \cdot \frac{d^2\left(T^{-1} \cdot i_g^{(dq)}\right)}{dt^2} + \underbrace{(L_g + L_2 + C_2 \cdot r^2)}_{a_1} \cdot \frac{d\left(T^{-1} \cdot i_g^{(dq)}\right)}{dt} - \underbrace{2 \cdot r \cdot i_g^{(\alpha\beta)}}_{a_0} \end{aligned} \quad (4.4)$$

The differential equation of grid-connected inverter in the d-q frame can be derived as:

$$\begin{aligned} v_c^{(dq)} &= a_3 \cdot \frac{d^3i_g^{(dq)}}{dt^3} + a_2 \cdot \frac{d^2i_g^{(dq)}}{dt^2} \\ &+ (a_1 - 3 \cdot a_3 \cdot \omega^2) \cdot \frac{di_g^{(dq)}}{dt} + (a_0 - a_2 \cdot \omega^2) \cdot i_g^{(dq)} \\ &+ \underbrace{(a_3 \cdot \omega^3 - a_1 \cdot \omega)}_K \cdot \begin{bmatrix} 0 & 1 \\ -1 & 0 \end{bmatrix} \cdot i_g^{(dq)} \end{aligned} \quad (4.5)$$

where K is the coefficient of the coupling network of the current loop. With the decoupling network, the coefficient is $-K$. The transfer function of $i_g(s)/v_c(s)$ can be found in:

$$\frac{i_g(s)}{v_c(s)} = \frac{1}{a_3 \cdot s^3 + a_2 \cdot s^2 + (a_1 - 3 \cdot a_3 \cdot \omega^2) \cdot s + (a_0 - a_2 \cdot \omega^2)} \quad (4.6)$$

Based on the transfer function, the PI current controller $G_{cig}(s)$ can be designed to reject the sinusoidal current into the grid. Fig. 4.1 shows the bode plots with and without using controller $G_{cig}(s)$. The original current loop has the gain at its resonant frequency. After using the controller, the magnitude of the resonance is around -20 dB which will decrease the oscillation of output voltage. The resistant of inductor is sensitive to the third transfer function.

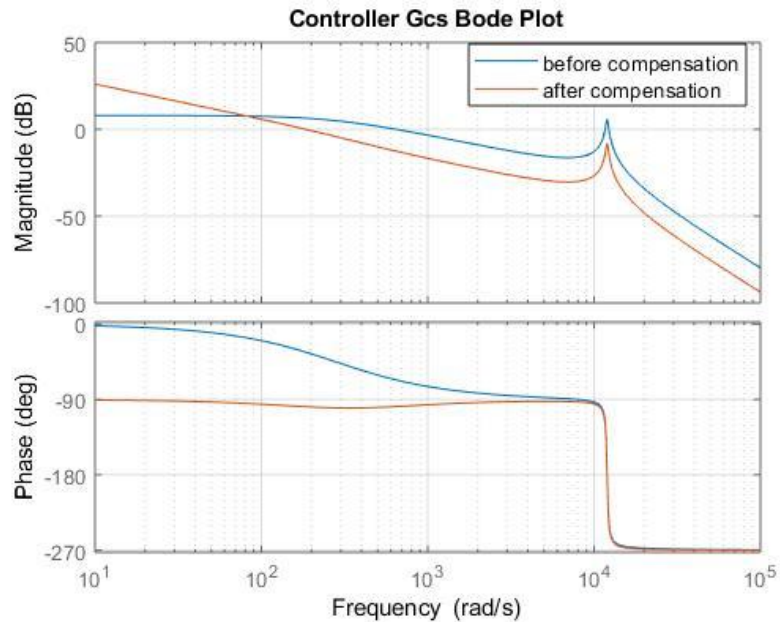


Fig. 4.1 Bode plots of inverter current loop with and without $G_{cig}(s)$.

4.1.2 System-level controller design in grid-connected mode

Fig. 4.2 shows the power flow of two inverters connected in parallel. $Z (= R + j \cdot X)$ and θ are the line impedance and its angle, respectively; δ is the phase angle difference between two inverters; U_1 and U_2 are the output voltage of two inverters, respectively.

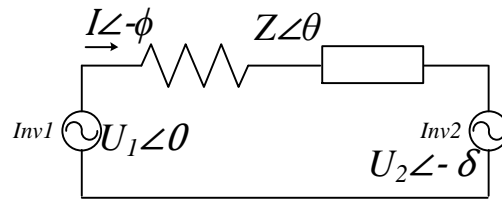


Fig. 4.2 The power flow between two inverters

The key method for the parallel operation of inverters is the droop control. It's widely used in power distribution systems. The advantage of droop control is that no external communication mechanism is needed among the inverters. And this is good for both linear and nonlinear loads sharing [31].

The inverter can be taken as a controllable energy source that regulates the frequency and the magnitude. The power generated by one inverter is:

$$\vec{S} = P + j \cdot Q = \vec{U}_1 \cdot \vec{I}^* = U_1 \cdot \left(\frac{U_1 - U_2 \cdot e^{j\delta}}{Z \cdot e^{-j\theta}} \right) = \frac{U_1^2}{Z} \cdot e^{j\theta} - \frac{U_1 \cdot U_2}{Z} \cdot e^{j(\theta+\delta)} \quad (4.7)$$

Therefore, the real power and reactive power can be found as follows:

$$\begin{cases} P = \frac{U_1}{R^2 + X^2} \cdot [R \cdot (U_1 - U_2 \cdot \cos \delta) + X \cdot U_2 \cdot \sin \delta] \\ Q = \frac{U_1}{R^2 + X^2} \cdot [X \cdot (U_1 - U_2 \cdot \cos \delta) - R \cdot U_2 \cdot \sin \delta] \end{cases} \quad (4.8)$$

then,

$$\begin{cases} U_2 \cdot \sin \delta = \frac{X \cdot P - R \cdot Q}{U_1} \\ U_1 - U_2 \cdot \cos \delta = \frac{R \cdot P + X \cdot Q}{U_1} \end{cases} \quad (4.9)$$

Since there is L_g in the inverter, $X \gg R$, then P and Q are proportional to δ and voltage difference, respectively. By adjusting the frequency and amplitude of the voltage, P and Q can be controlled independently. In the d-q frame, $Q = V_q \cdot I_d - V_d \cdot I_q$, specially when the synchronous frame is align to V_d , $V_q = 0$, then the following droop controller can be designed as follows:

$$\begin{cases} f = f_0 - k_p \cdot P \\ I_q^* = 0 - k_q \cdot Q \end{cases} \quad (4.10)$$

where k_p and k_q are droop coefficients corresponding to P and Q , respectively; f_0 is the reference frequency. I_q^* is the reference current of i_q . Fig. 4.3 shows the conventional droop control. The parallel connected inverters can be controlled in parallel to meet the same conditions, which means the output voltage, frequency and phase in consistently.

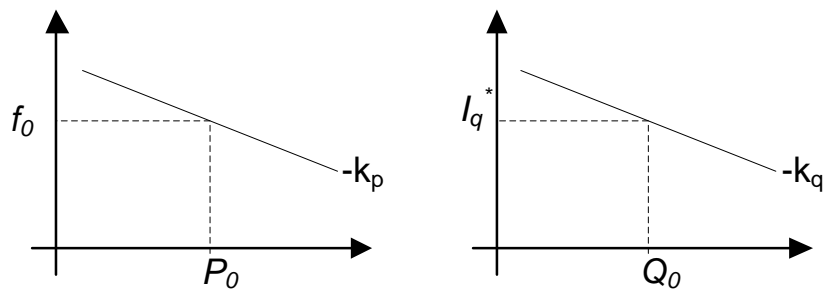


Fig. 4.3 droop control

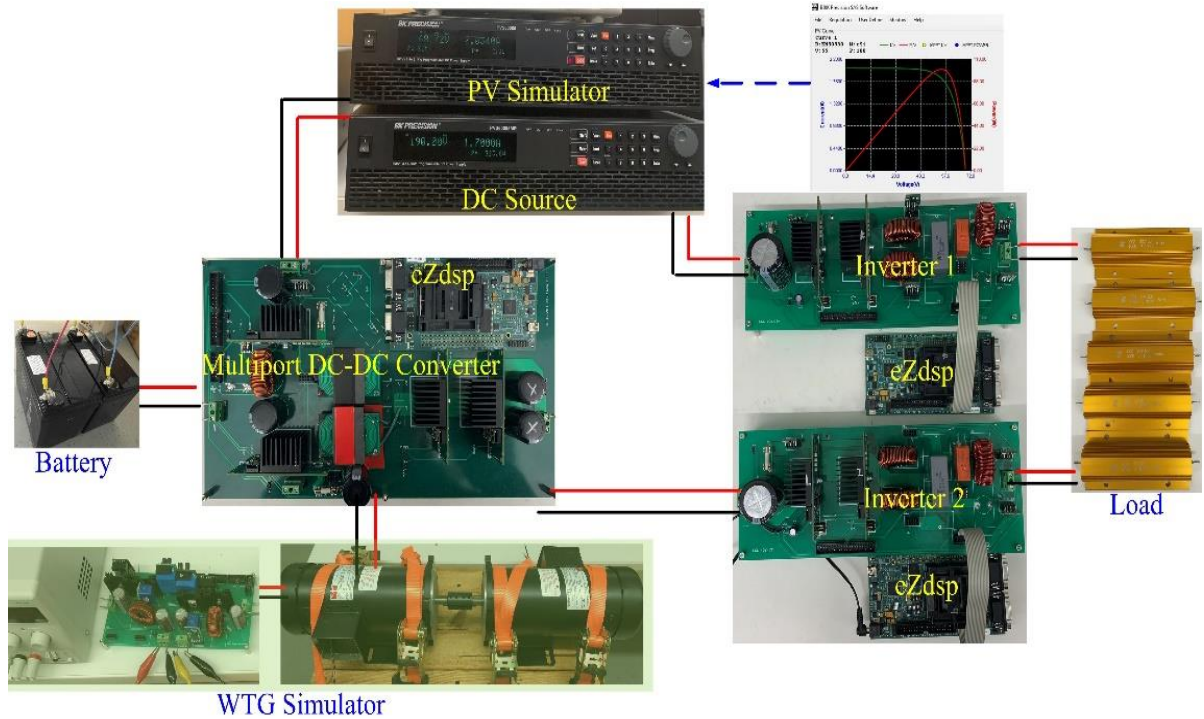


Fig. 4.5 Experiment setup

4.2.1 Setup with microprocessor board

Any continuous and time-varying signal, such as voltage, current and voice, is an analog signal. By contrast, a set of discrete or finite signal is called digital signal. Working with electronics needs to deal with both analog and digital signals. In this work, all the converters connect with the digital signal processing (DSP) board which is implemented with chip TMS320F28335. The code is firstly programmed in Matlab Simulink. After building the code, the code can be loaded into the DSP processor by IDE software code composer studio (CCS). Fig. 4.6 shows the setup in CCS.

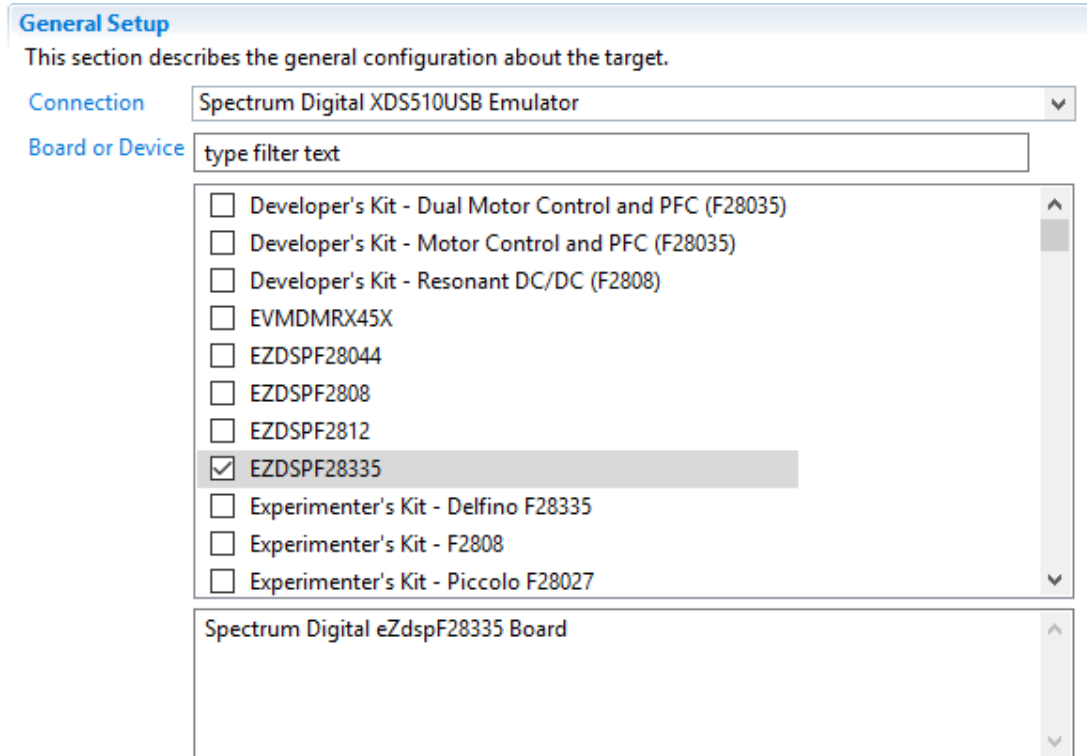


Fig. 4.6 Set up for DSP in CCS

In order to process the analog and digital signals, an analog to digital converter (ADC) is a useful feature that converts an analog voltage or current to a digital value. Typically, the digital output value is proportional to the input. For F28335 DSP, it has two ports and eight pins for each port to do ADC conversion. And the ADC is 12-bit which means it can detect 4096 discrete analog values. In this system, the maximum system voltage is 3 V. This means that the ADC assumes 3 V is 4095 and anything less than 3 V will be a ratio between 0 and 4095. Thus, the equation can simply describe as follows:

$$D = \frac{4095}{3} \cdot A \quad (4.11)$$

The sampling for the voltage is based on the voltage divided circuit. So, the sampling value of voltage can be written as:

$$V_u = \frac{R_6}{R_4 + R_5 + R_6} \cdot V_{real} \quad (4.13)$$

where R_4 , R_5 and R_6 are the resistances which can be chosen by the requirement. In this work, the maximum real voltage through the inverter is 200 V. And take the power consumption into consideration. The R_4 , R_5 and R_6 are chosen as 100k, 100k and 1.5k respectively.

However, the controllers need to control the real analog values. The sampling values will be converted into real values after the ADC. In order to get the real values of current or voltage, the coefficient is reserve to the sampling one. Fig. 4.8 shows the example of voltage sampling signal which reads directly from DSP. It has the spikes at high frequency. It's related to the calculation in the ADC. To reduce this, one way is to improve the accuracy by decreasing the sampling time T_s . The more sensed points in one period, the more accurate sampling signal will get. Meanwhile, it requires more data space for the calculation. In order to build d-q frame in this work, time delayed method is adopted which uses the delay block to store the data. Therefore, it has to keep balance between the number of sensed signals and storage. In this work, the T_s is 52 microseconds.

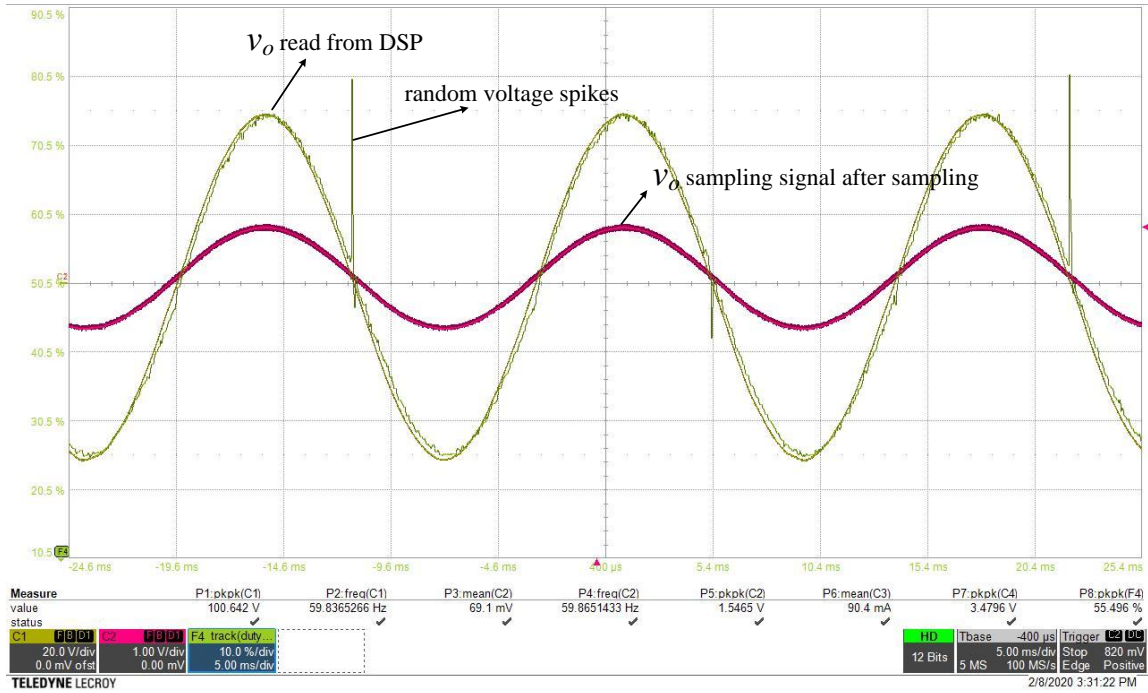


Fig. 4.8 Original voltage sampling signals

Another way to reduce the spikes or the oscillation is to add filter. The spikes occurs at high frequency. So the RC low pass filter can be used. Fig. 4.9 shows the RC circuit for filter.

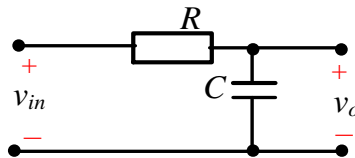


Fig. 4.9 RC low pass filter circuit

The transfer function of LPF can be derived as follows:

$$H(s) = \frac{1}{R \cdot C \cdot s + 1} \quad (4.14)$$

The code in Matlab to get the discrete transfer function is shown as follows:

$$\tau = 1 / (2 \cdot \pi \cdot f_c) \quad G = tf(1, [\tau \ 1]) \quad z = c2d(G, T_s, 'zoh') \quad (4.15)$$

where the f_c is the cut off frequency for the filter, $c2d$ is the function to transfer the continuous to the discrete in Matlab. In this work, the cut off frequency of the filter can be chosen at 15 kHz. Fig. 4.10 shows the sampling voltage of inverter using a 15 kHz filter.

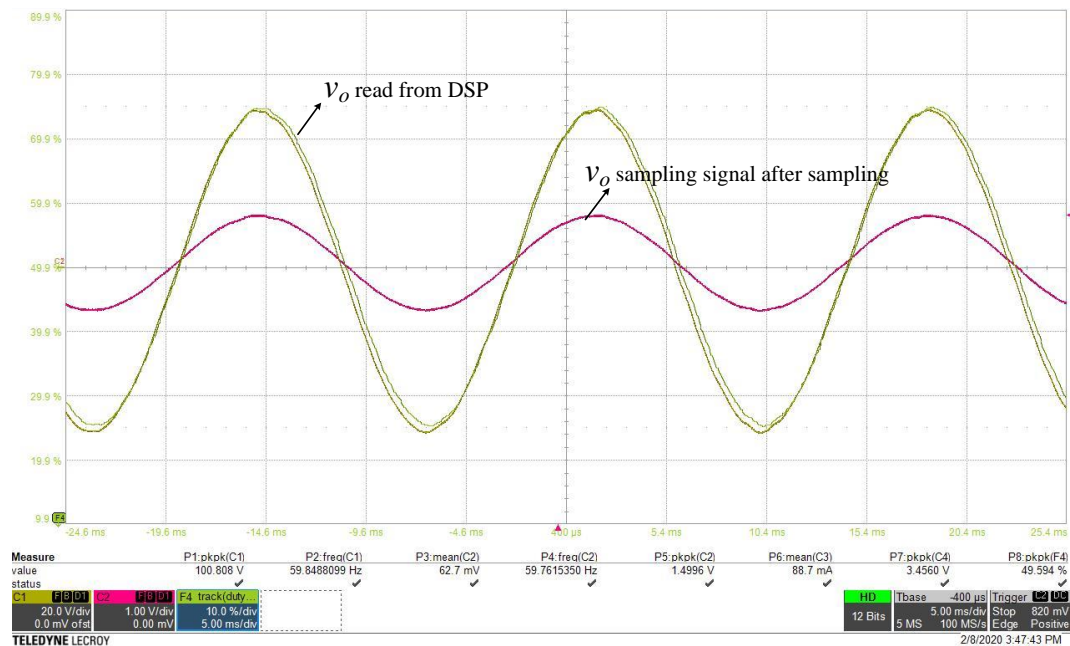


Fig. 4.10 Voltage sampling signals using the LPF filter.

The sampling signal is consistent with the real signal without any spikes. The accuracy of the ADC and sampling is the key to d-q transformation and controllers. Therefore, the check for sampling signals is the first thing to do.

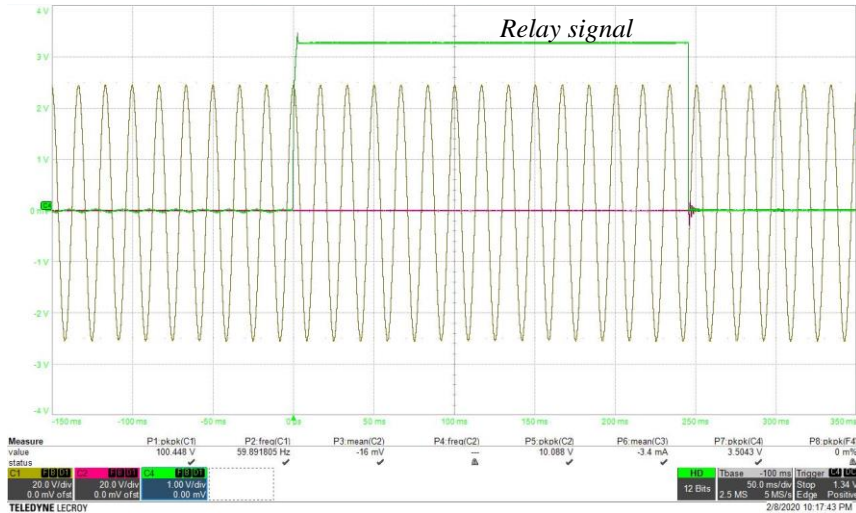


Fig. 4.12 The initialization of relay signal

However, the relay has delay time to close. It's important to get the right time for the relay closed. Otherwise, the synchronization may have errors. Fig. 4.13 shows the time for relay closing. It takes around 12 microseconds. When the inverter is in phase with the grid, the droop controller will be ready to do the power sharing.

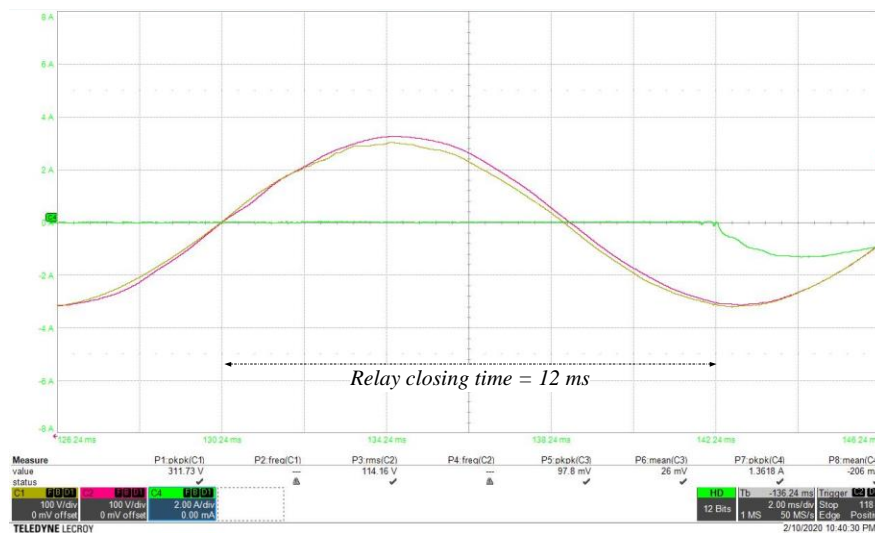


Fig. 4.13 Time for relay closed

Fig. 4.14 shows the overall sequence of experiment. Before connecting with the grid, one inverter can output stable waveforms. And the PLL block will be used to detect the zero-crossing for synchronization. The relay will be closed when the new inverter can work stably with same grid angle. Then the droop control is for power sharing.

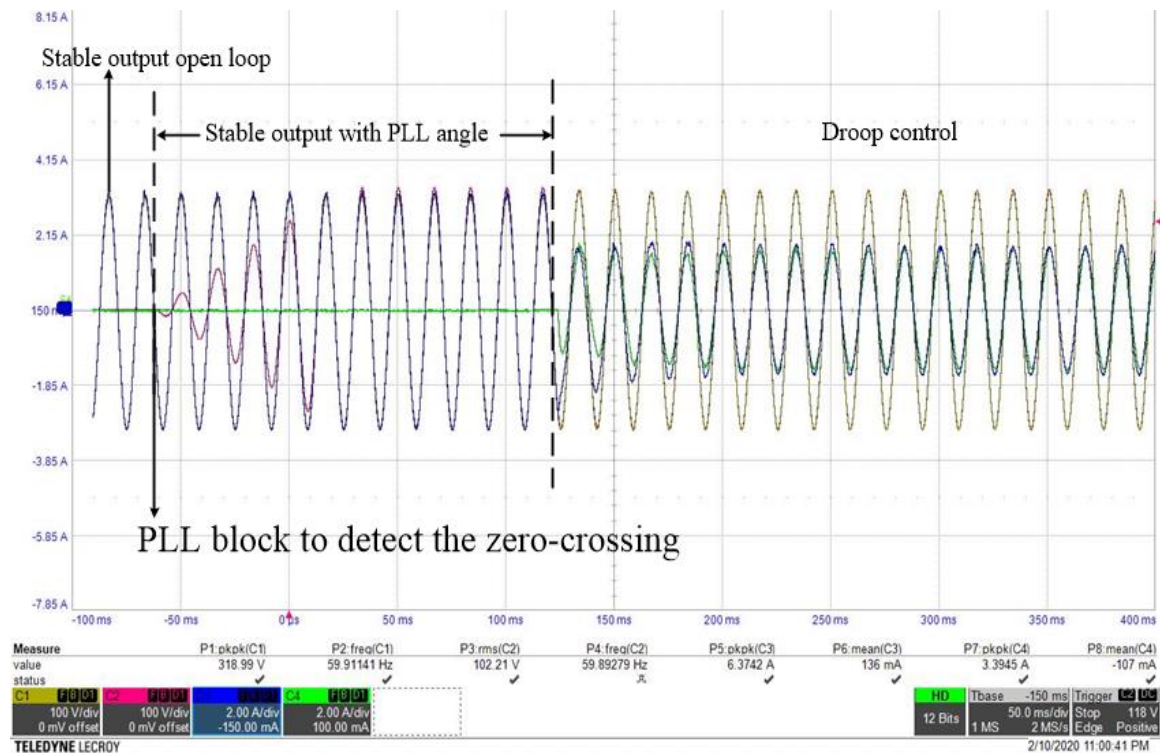


Fig. 4.14 Sequence for grid connection

4.3 Experimental results and analysis

After the setups, the experiment can be carried out to verify the inverter working in the grid connected mode.

4.3.1 Steady response in grid-connected mode

Fig. 4.15 shows the steady-state waveform when the inverter works in the grid connected mode. i_{g1} and i_{g2} are the output current of two parallel connected inverters. The output voltage is 110V with 60 Hz. The mean value of DC-link voltage V_{dc} is controlled to be 190 V. The currents are in phase with v_g and the magnitude is close, i.e., i_{g1} and i_{g2} which peak-to-peak values are 3.43 A and 3.46 A, respectively. This indicates two units are sharing power equally.

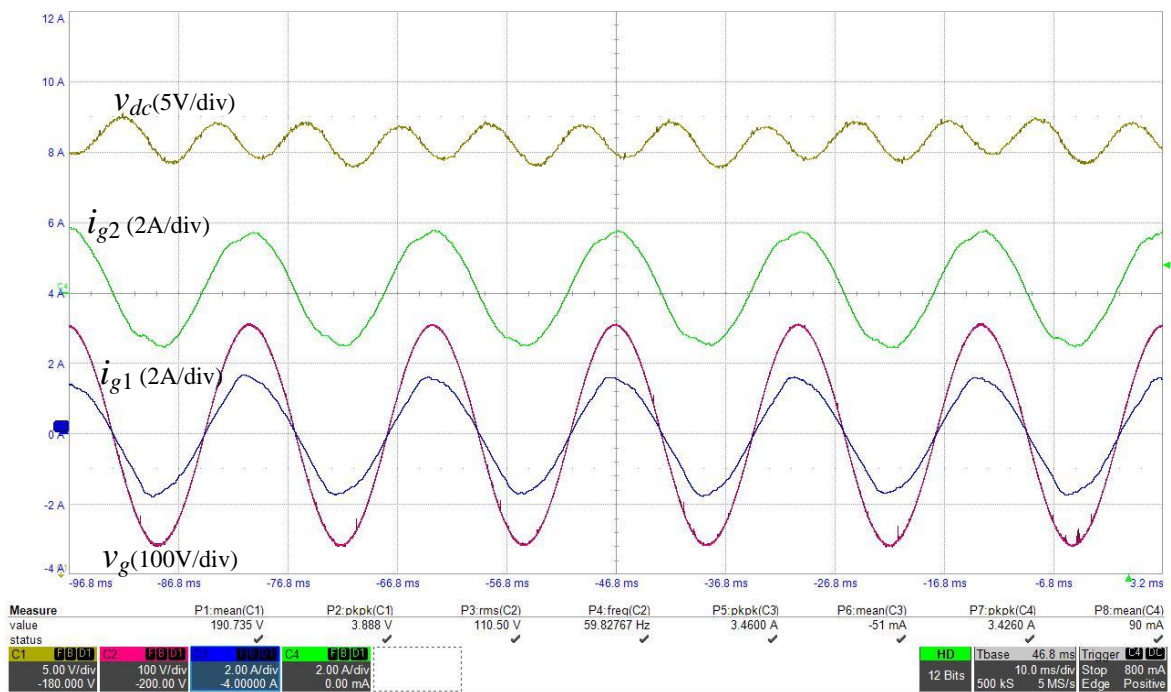


Fig. 4.15 Steady-state waveforms with grid

4.3.2 The transient responses with grid

To test the dynamic of the system, Fig. 4.16 shows the measured transient waveforms when the inverter is connected to the grid. At first, the load is supplied by one

inverter. The peak-to-peak value of i_{g1} is 6.4 A. When the other inverter is connected at $t = 255$ ms, i_{g1} decreases and i_{g2} increases. The peak-to-peak value of i_{g2} is increased to 3 A within 100 ms. The output voltage is around 110 V and frequency is around 60 Hz.

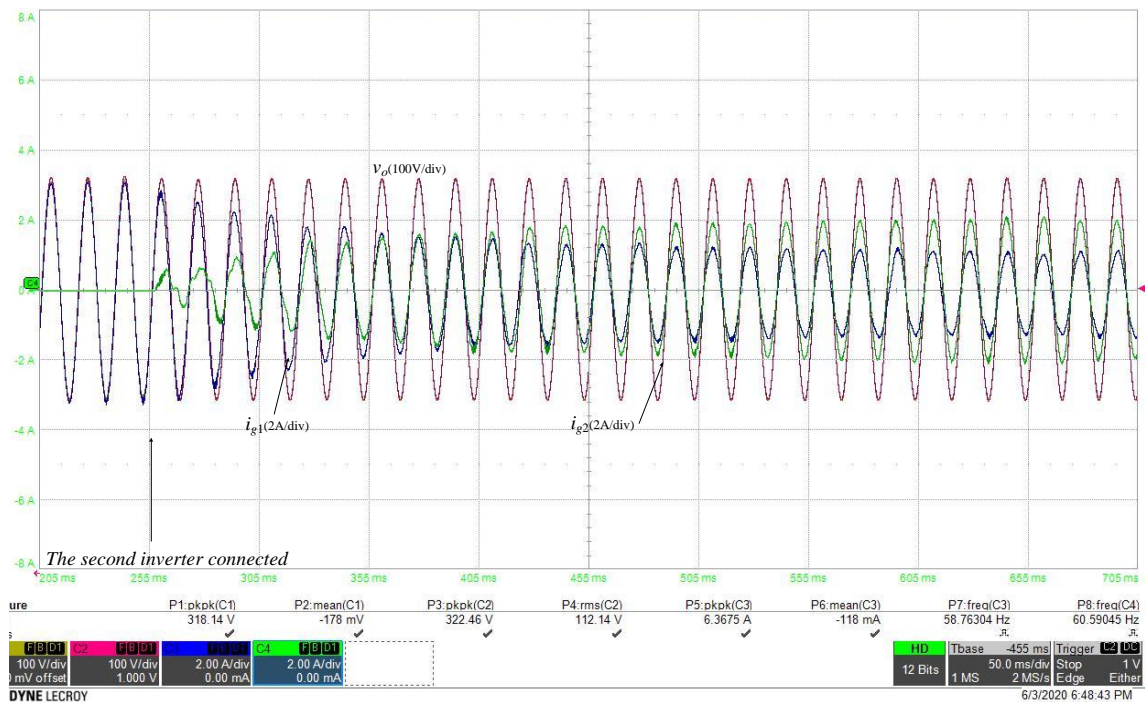


Fig. 4.16 Dynamic waveforms when the inverter connected with the grid

Fig. 4.17 shows the waveforms that the inverter is switched from grid connected mode to the standalone mode. Both inverters supply the power to the load at the beginning, then one inverter is removed at $t = 0$. Therefore, $i_{g1} = 0$ and the current of the other inverter i_{g2} increases quickly to supply the load power. The DC-link voltage drops to 178 V and then goes back to normal. V_{dc} is still controlled to be 190 V. The whole transient lasts around 100 microseconds. But the output voltage is controlled to be 110 V AC during the whole transient.

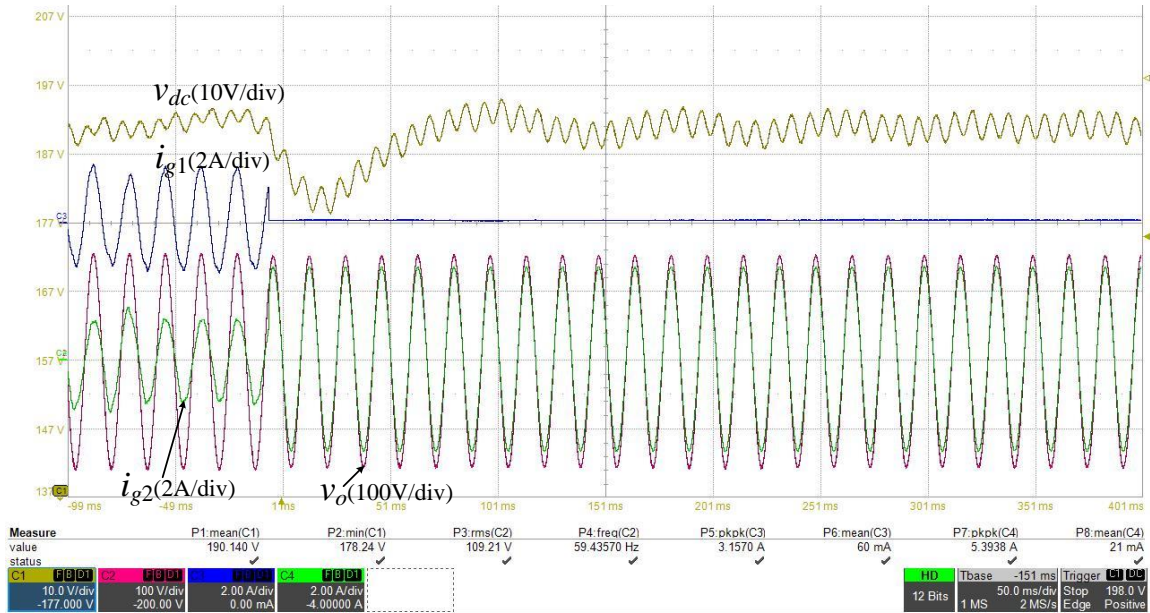


Fig. 4.17 Waveforms that one inverter disconnected with grid

Fig. 4.18 shows the waveforms for the load changing from 100Ω to 50Ω . The waveforms are similar with the mode switch. During the transient, v_{dc} is controlled between 186 V and 194 V. The output voltage is controlled to be 110 V AC too. When the load is changed to 50Ω , the current of both inverter increases which means the inverters can share the power after the load change.

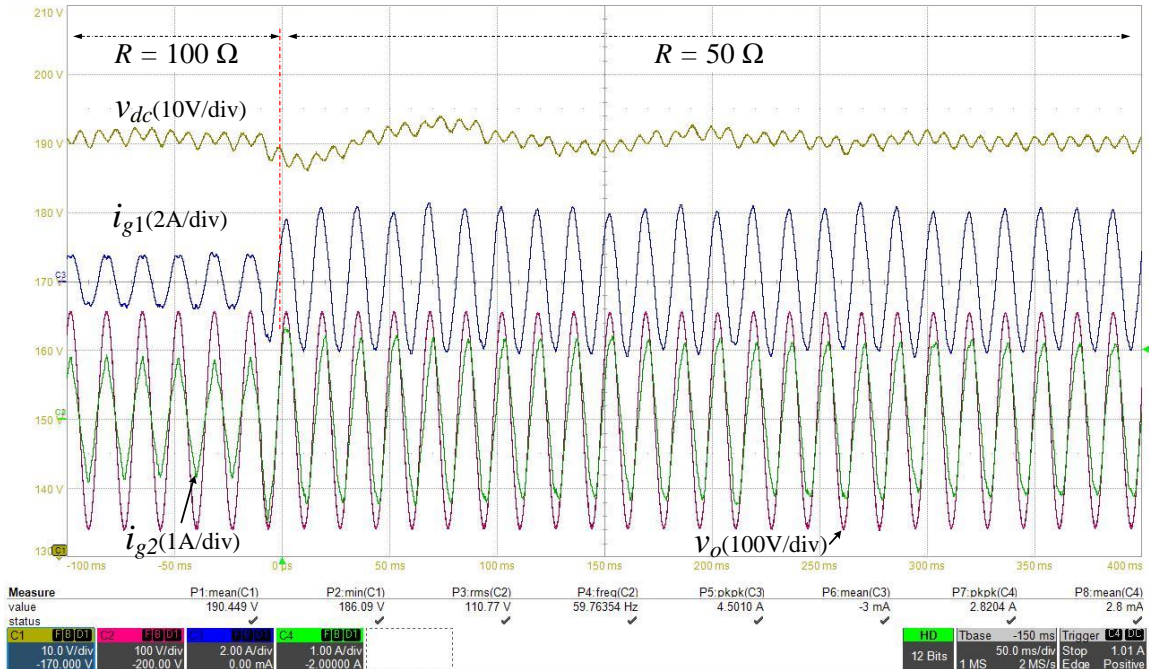


Fig. 4.18 Waveforms when the resistive load is changed from 100Ω to 50Ω

4.3.3 Quality analysis of the inverters

The quality of current is measured by THD. The equation to calculate the THD for the current is:

$$THD = \frac{\sqrt{\sum_{n=2}^{\infty} i_{n_RMS}^2}}{i_{1_RMS}} \quad (4.16)$$

where n is the numbers of the integer multiples of the frequency of the main signal, i_{1_RMS} is the RMS current of the fundamental frequency which is 60 Hz.

Fig. 4.19 shows the spectrum of current i_{g1} at steady state. Compared to the amplitude at fundamental frequency, the amplitude at second and third harmonic frequency

is much lower, which is 21.25 mA and 19.12 mA respectively. And the calculated current THD is 3.97% which is less than 5%.

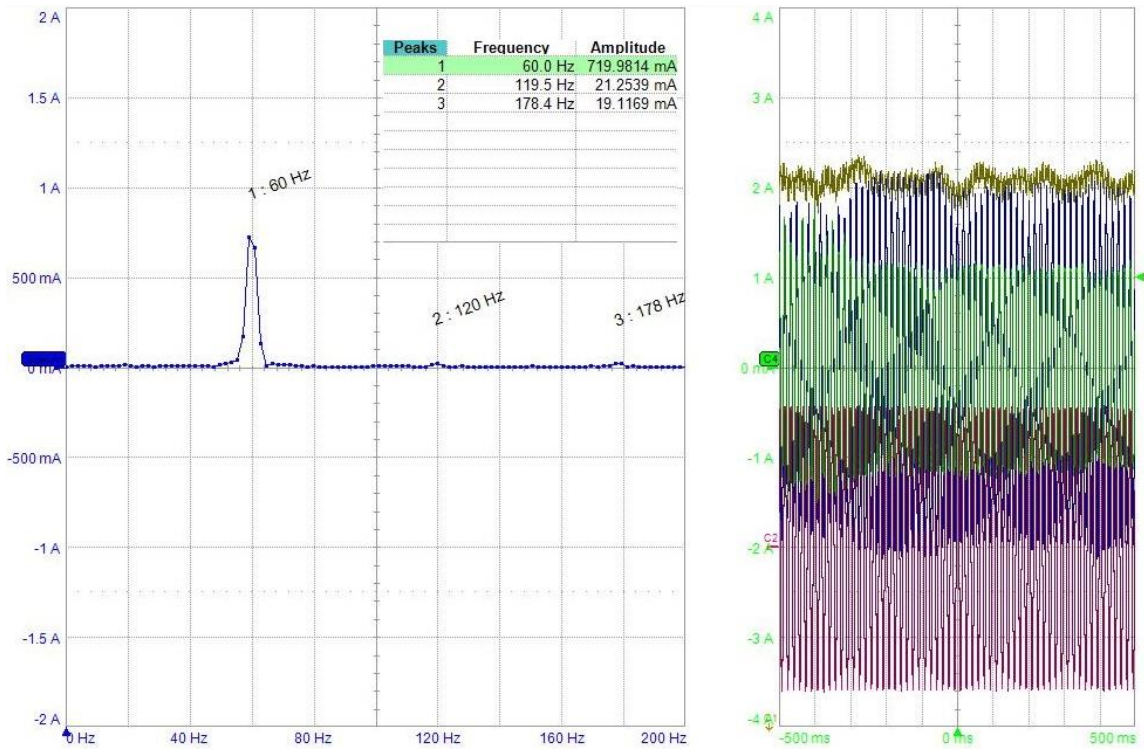


Fig. 4.19 Spectrum of the current i_g .

Chapter 5 Conclusions and Recommendations for Future Works

5.1 Conclusions

The objective of this thesis is to develop multiport converters for renewable energy integration and microgrid application. The proposed converters have the advantages of using less ports to integrate different types of renewable energy sources and working with and without the grid. In this thesis, the single-phase inverter was proposed, designed and validated by the experimental results. They were:

- ❖ Controller design in the d-q frame.
- ❖ Synchronization with the grid.
- ❖ Droop controller for power sharing.
- ❖ Stable work at standalone mode, grid-connected mode and switched mode.

The controller design of the proposed inverter is based on the d-q transformation. In this approach, the AC signals can be transferred into “dc” variables in the synchronous frame. Therefore, it can simplify the complexity of calculation. And, it is easier to be controlled and only two regulator structures are required, in the d and q axes only. The experiment showed that the inverter implemented with controllers in d-q frame can output stable sinusoid waveforms.

The proposed inverter is designed to synchronize with the grid. When it connected with the grid, the inverter can detect the zero-crossing point and read the phase from the

grid. Then relay can be set to connect the inverter and grid. The experimental results showed that the inverter voltage and grid voltage are in phase before the relay closing.

Droop controller is used to distribute the power when the inverter is connected with the grid. In this work, experimental results showed that the power for inverters can be shared equally.

The proposed inverters can work at standalone mode and grid connected mode. The experimental results were provided to show the steady response and dynamic states. The inverter can also work at switched mode, such as switched from standalone mode to grid connected mode, disconnected with grid mode and load changing mode.

A new two-level control of a two-stage four-port DC-AC inverter was proposed for integrating with the grid with different energy sources. Simulation and experimental results showed that the inverter was capable of working and switching from grid connected mode and the standalone mode.

5.2 Recommendations for future work

Recommendations for future work are listed as follows:

Improve the initialization of current: When the inverter connected with grid, the current has a delay. And it takes some period to be stable.

Power sharing: The inverter can work stably and share the power equally when the load is resistive. It will be worthwhile to investigate the droop controllers for different power sharing ratios with different types of load.

Appendix

The .m file in Matlab Simulink:

```

% Param
f = 100e3; %f for PWM
Ts = 52e-6; % sampling freq., 50 kHz
Tctrl = Ts;
fg = 60.0962; T = 1/fg;
N = T/Ts;
N = 320;

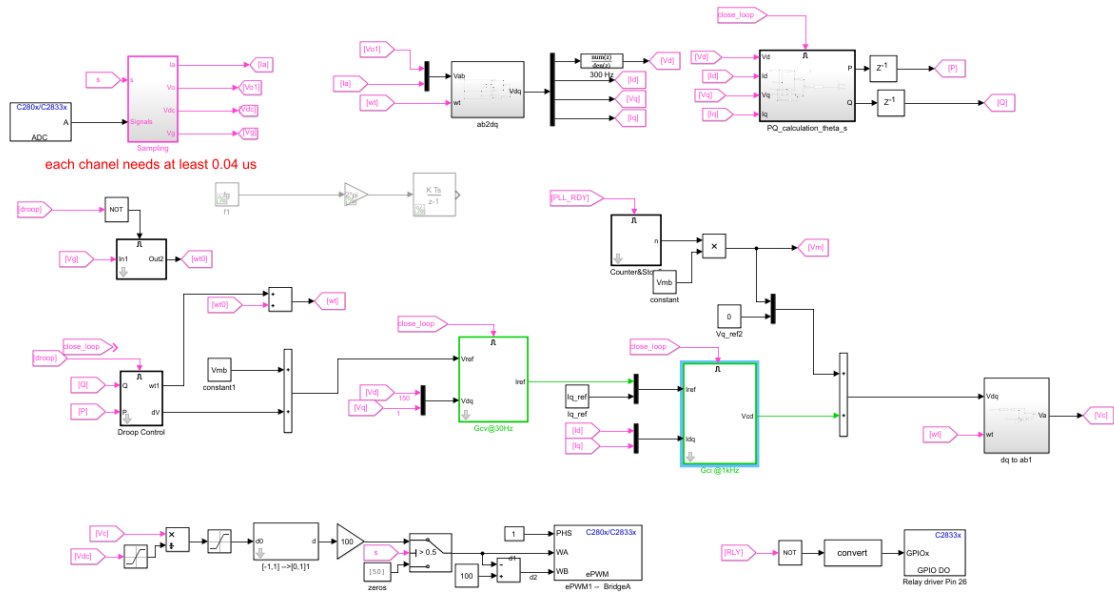
N1 = 8*N; % delay 8T for close loop
N2 = 2*N; % delay 2T for getting Vmax
NRLY = ceil(7.5e-3/T*N); % takes 12 ms to close

C2 = 22e-6;
L2 = 2*(480e-6); % INV inductance
w = 2*pi*fg;
Vdc = 190;
Vm = 158;
Vmb = Vm ;
%% just input the slope ONLY
kia = 8.5; %5A
kv = 67;
% voltage loop
Kp1 = 4e-3; Ki1 = 8.7; % fc = 30 Hz
Imax = 6;
% current loop
Kp2 = 6.4; Ki2 = 400; % fc = 1kHz
Vmax = [2];
%% P & Q filter
ap = 0.0194; bp = 1- ap; % 60 Hz

Q0 = Vm^2*w*C2/2;
P0 = Vm^2/100/2/2;
Iq_ref = w*C2*Vm;
Max_dV = 0.4;
% droop control
kp = Max_dV / (P0);
kq = 0.39 / (Q0);
return;
% filter param
Ti = 1/(2*pi*1e3); Gi = tf(1,[Ti 1]); z10k = c2d(Gi,Ts,'zoh');

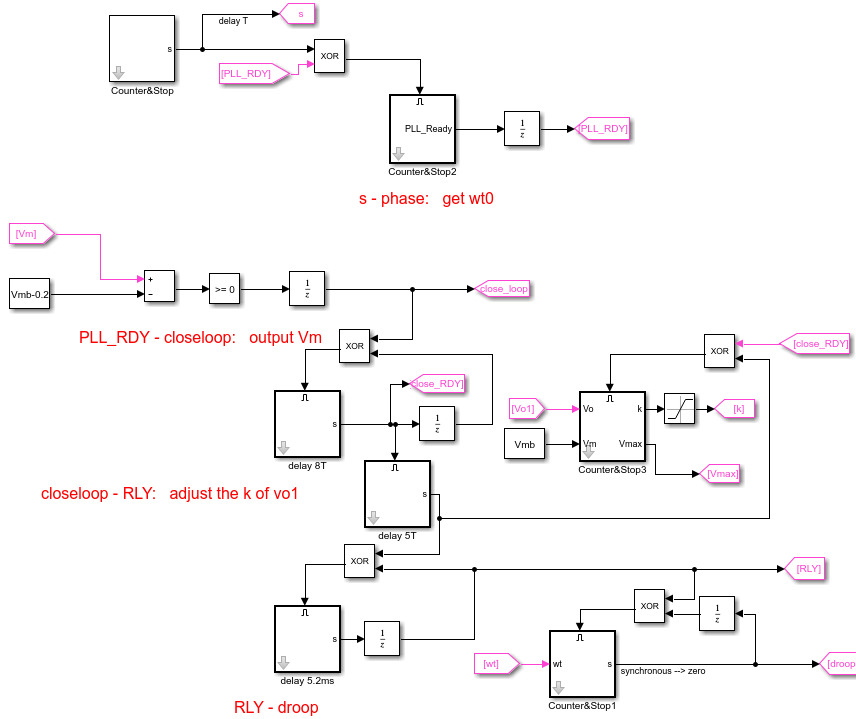
```

The signal flows in Matlab Simulink block:



each channel needs at least 0.04 us

The time sequence blocks:



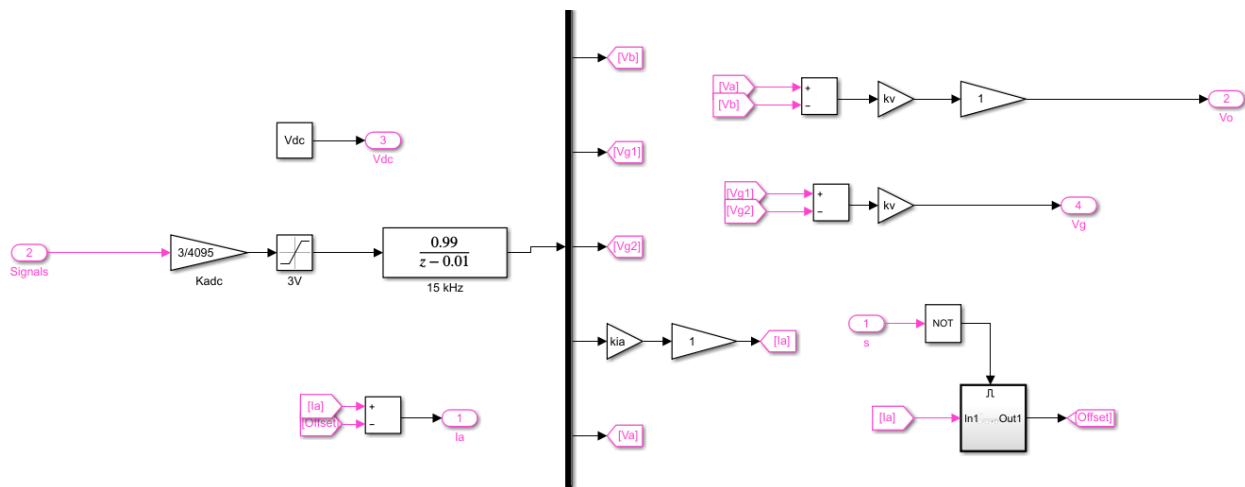
s - phase: get wt0

PLL_RDY - closeloop: output Vm

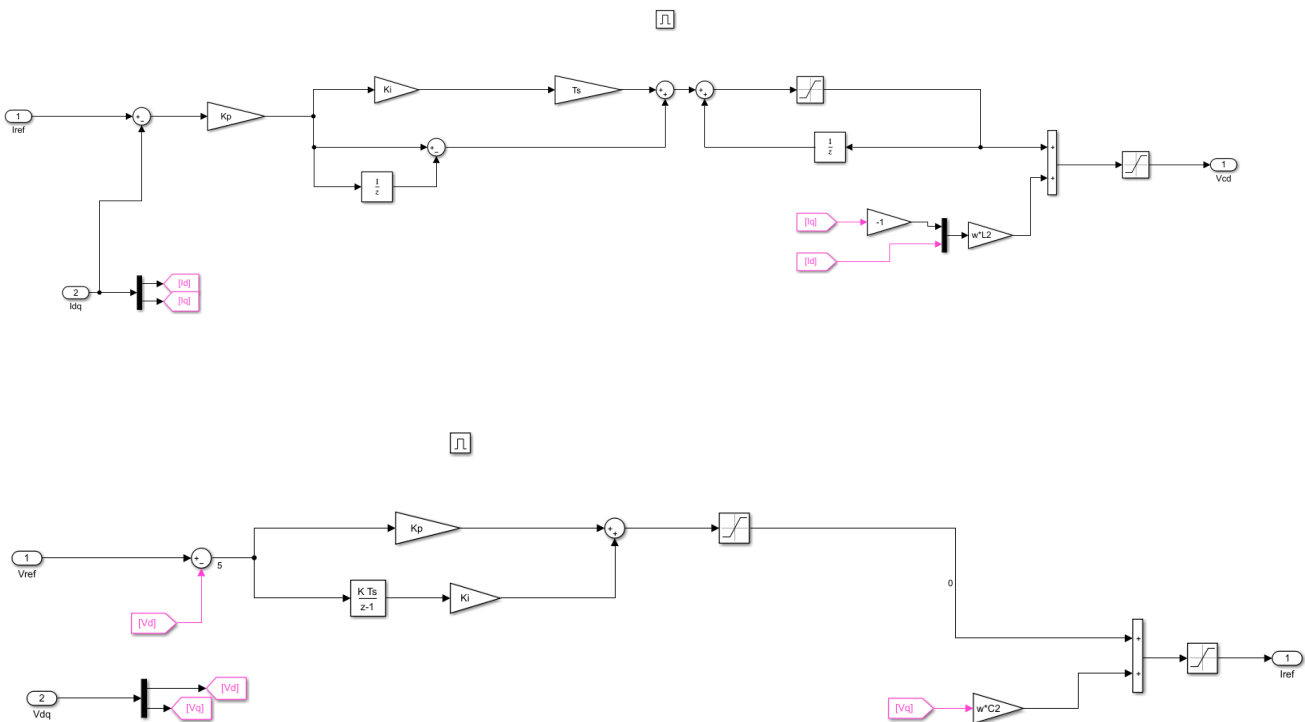
closeloop - RLY: adjust the k of vo1

RLY - droop

Sampling block:



Controller block:



Parameters in controller block:

Block Parameters: Gcv@30Hz

Subsystem (mask)

Discrete PI controller with:

$$\frac{Kp(s+Ki)}{s(s+p)}$$

Parameters

Portional parameter (Kp)

Kp1

Integral parameter (Ki)

Ki1

Poles

0

Sample Time (Ts)

Ts

Upper Limiter (Max)

Imax

Lower Limiter (Min)

-Imax

OK Cancel Help Apply

Filter block:

Block Parameters: Filtrt@60Hz

Discrete Transfer Fcn

Implement a z-transform transfer function. Specify the numerator and denominator coefficients in descending powers of z. The order of the denominator must be greater than or equal to the order of the numerator.

Main Data Types State Attributes

Data

	Source	Value
Numerator:	Dialog	[ap]
Denominator:	Dialog	[1 -bp]
Initial states:	Dialog	0

External reset: None

Input processing: Elements as channels (sample based)

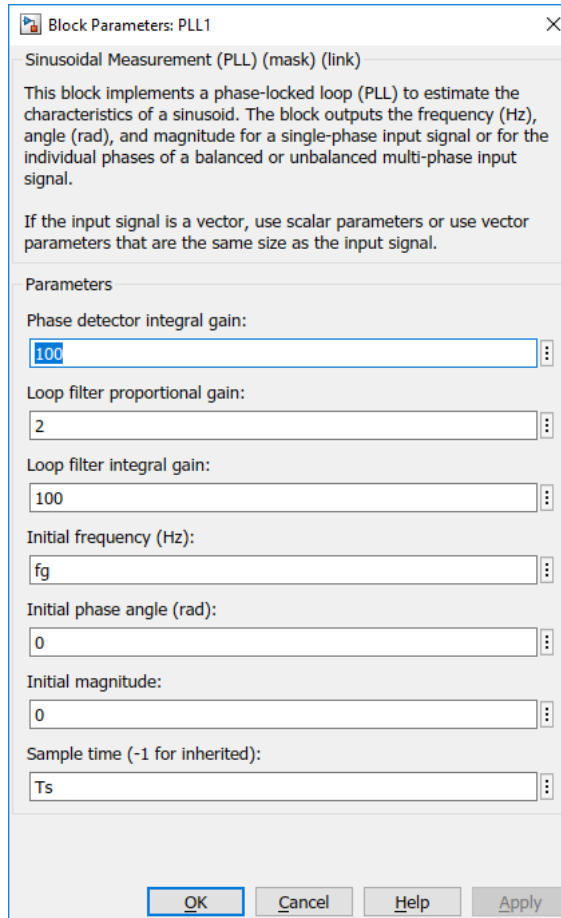
Optimize by skipping divide by leading denominator coefficient (a0)

Sample time (-1 for inherited):

Ts

OK Cancel Help Apply

Parameters in PLL Block:



Functions to design PI controller and get the bode plots:

```
Vdc = 190; R = 22; C2 = 22e-6; L2 = 2*(480e-6); r2 = 2*0.1;
L = 1e-3; Vm = 110*sqrt(2);
w = 2*pi*60; Rd = 0.5; Lg = 470e-6;
% V(s)/I(s)
Gv = tf(R, [R*C2, 1])
% ia(s)/ d(s)
Gi = tf([1], [L2, r2]);
% ig(s)/Vc(s)
Gs = tf([1], [L2*Lg*C2, (L2+Lg)*C2*r2, (L2+Lg)+C2*r2^2-3*L2*Lg*C2*w^2,
2*r2-(L2+Lg)*C2*r2*w^2]);
% controller design
Gcs = 0.2*tf([1, 400], [1, 0]); %LCL
Gcv = 4e-3*tf([1, 8.7], [1, 0]); %LC
Gci = 0.04*tf([1, 200], [1, 0]);
```

```
% H(s) -- sample circuit LPF R = 10.2e3;C = 4.7e-9;
R2 = 10.2e3;C = 4.7e-9;
H = tf(1,[R2*C 1]);
return;

% compensation Ia
bode(Gs);
hold on;
bode(Gs*Gcs);
title('Controller Gcs Bode Plot');
legend('before compensation','after compensation');
h = legend('before compensation','after compensation');
set(h,'FontSize',10);
grid on;

% compensation Vc
bode(Gv);
hold on;
bode(Gv*Gcv);
title('Controller Gcv Bode Plot');
legend('before compensation','after compensation');
h = legend('before compensation','after compensation');
set(h,'FontSize',10);
grid on;

% % compensation ia
bode(Gi);
hold on;
bode(Gi*Gci);
title('Controller Gci Bode Plot');
legend('before compensation','after compensation');
h = legend('before compensation','after compensation');
set(h,'FontSize',10);
grid on
```

References

- [1] L. Che, M. Khodayar, and M. Shahidehpour, “Only connect: Microgrids for distribution system restoration,” *IEEE power & energy magazine january*, Jan./Feb. 2014.
- [2] K. Surendra, and C. Vyjayanthi, “Fault Level Analysis in Modern Electrical Distribution System Considering Various Distributed Generations,” 2018 *International Conf. on Power, Energy, Control and Transmission Systems (ICPECTS)*, Chennai, pp. 36-42, Nov. 2018.
- [3] S. Abu-Elzait, and R. Parkin, “Economic and Environmental Advantages of Renewable-based Microgrids over Conventional Microgrids,” *IEEE Green Technologies Conference (Green Tech)*, Lafayette, LA, pp. 1-4, Jul. 2019.
- [4] J. Zeng, “Isolated Mutiport Converters for Renewable Energy Conversion and Microgrids,” Jan. 2015.
- [5] T. Funabashi, “Integration of Distributed Energy Resources in Power System,” 2016.
- [6] H. Jo, J. Kim, G. Byeon and S. Kim, “Optimal Scheduling Method of Community Microgrid with Customer-owned Distributed Energy Storage System,” 2019 *International Conf. on Smart Energy Systems and Technologies (SEST)*, Porto, Portugal, pp. 1-6, Sep. 2019.
- [7] “Electrical energy storage technology options,” Report 1020676, Electric Power Research Institute, Palo Alto, CA, Dec. 2010.
- [8] M. Alramlawi, Y. Souidi and P. Li, “ Optimal Design of PV-Battery Microgrid Incorporating Lead-acid Battery Aging Model,” 2019 *IEEE International Conf. on Environment and Electrical Engineering and 2019 IEEE Industrial and Commercial Power Systems Europe (EEEIC / I&CPS Europe)*, Genova, Italy, pp. 1-6, Aug. 2019.

- [9] A. Vukojevic, "Lessons Learned from Microgrid Implementation at Electric Utility," 2018 *IEEE Power & Energy Innovative Smart Grid Technologies Conf. (ISGT)*, Washington DC, pp. 1-5, Jul. 2018.
- [10] L. Che, M. Shaidehpour, A. Alabdulwanhab, and Y. Al-Turki, "Hierarchical coordination of a community microgrid with AC and DC microgrids," *IEEE Transactions on Smart Grid*, vol. 6, no. 6, Nov. 2018.
- [11] J. Zeng and W. Qiao, "Short-term wind power prediction using a wavelet support vector machine," *IEEE Trans. Sustainable Energy*, vol. 3, pp. 255-264, April 2012.
- [12] X. Peng, W. Fan, F. Yang, J. Che and B. Wang, "A Short-term Wind Power Prediction Approach Based on The Dynamic Classification of The Weather Types of Wind Farms," 2017 *China International Electrical and Energy Conference (CIEEC)*, Beijing, pp. 612-615, Jun. 2018.
- [13] J. Zeng and W. Qiao, "Short-term solar power prediction using an RBF neural network," in *Proc. Power and Energy Society General Meeting*, Detroit, July 2011, pp.1-8.
- [14] Y. Zhang, S. Gao, J. Han and M. Ban, "Wind Speed Prediction Research Considering Wind Speed Ramp and Residual Distribution," in *IEEE Access*, vol. 7, pp. 1 31873-131887, Sept. 2019.
- [15] J. Zeng and W. Qiao, "Short-term solar power prediction using a support vector machine," *Renewable Energy*, vol. 52, pp. 118-127, April 2013.
- [16] J. Pomilio and G. Spiazzi, "A double-line-frequency commutated rectifier complying with IEC 1000-3-2 standards," in *Proc. Appl. Power Electron. Conf. Exposit.*, pp. 349-355, Mar. 1999.
- [17] H. Jou, J. Huang, J. Wu and K. Wu, "Novel Isolated Multilevel DC-DC Power Converter," in *IEEE Transaction on Power Electronics*, vol. 31, no. 4, pp. 2690-2694, Apr. 2016.

- [18] D. Kumar, Amarnath, R. Jain and R. K. Singh, "Comparison of Non-Isolated Boost Converter & Isolated Flyback Converter for PV Application," 2017 *International Conf. on Innovations in Control, Communication and Information Systems (ICICCI)*, India, pp. 1-7, Aug. 2017.
- [19] R. Zhao and A. Kwasinski, "Efficiency improvement of a low-power multiple-input converter with forward-conducting-bidirectional-blocking switches," in *Proc. IEEE Energy Convers. Congr. Exposit.*, pp. 5566-5573, Sept. 2013.
- [20] K. Sayed, M. Abdel-Salam, A. Ahmed, and M. Ahmed, "New high voltage gain dualboost DC-DC converter for photovoltaic power system," *Electric Power Components and Systems*, vol. 40, no. 7, pp. 711-728, Apr. 2012.
- [21] M. A. Salvador, T. B. Lazzarin and R. F. Coelho, "High Step-up DC-DC Converter with Active Switched-inductor and Passive Switched-capacitor Network," *IEEE Trans. on Industrial Electronics*, vol. 65, no. 7, pp. 5644-5654, Jul. 2018.
- [22] S. Lu, L. Yuan, N. Xie and D. Yu, "Zero Ripple High-Gain DC/DC Converter Based on Switched Capacitor Network," in 2019 4th *International Conf. on Intelligent Green Building and Smart Grid (IGBSG)*, Hubei, Yi-chang, China, pp. 616-622, Oct. 2019.
- [23] M. Forouzesh, Y. Shen, K. Yari, Y. P. Siwakoti and F. Blaabjerg, "High-efficiency High Step-up DC-DC converter with Dual Coupled Inductors for Grid-connected Photovoltaic Systems," *IEEE Trans. on Power Electron.*, vol. 33, no. 7, pp. 5967-5982, Jul. 2018.
- [24] S. Chen, T. Liang, L. Yang, and J. Chen, "A cascaded high step-up DC-DC converter with single switch for microsource applications," *IEEE Trans. Power Electron.*, vol. 26, no. 4, pp. 1146-1153, Apr. 2011.
- [25] F. Blabjerg, "Control of Power Electronic Converters and Systems," 2018.
- [26] Y. Zeng, "Droop Control of Parallel-Operated Inverters," Jun. 2015.

- [27] B. Crowhurst, E.F. El-Saadany, L. El Chaar, and L.A. Lamont, "Single-phase grid-tie inverter control using dq transform for active and reactive load power compensation," *IEEE International Conf. on Power and Energy*, Nov. 2010.
- [28] R. S. Kushwah, and G. R. Walke, "Parallel Operation of Inverters with Droop Control of Voltage and Frequency," 2018 *International Conf. on Smart City and Emerging Technology (ICSCET)*, pp. 1-5, Nov. 2018.
- [29] S. Jayalath, and M. Hanif, "Generalized LCL-filter design algorithm for grid-connected voltage-source inverter," *IEEE Trans. of Industrial electronics*, vol. 64, no. 3, pp. 1905-1914, Mar. 2017.
- [30] P. Mao, M. Zhang, S. Cui, W.Zhang, and B.Kwon, "A review of current strategy for single-phase grid-connected inverters," *TELKOMNIKA*, vol. 12, no. 3, pp. 563–580, Sep. 2014.
- [31] Anuroop.P.V, K. Radhakrishnan, and A.S. Kumar, "Droop control of parallel inverters with LCL filter and virtual output impedance," *International Journal of Advanced Research in Electrical, Electronics and Instrumentation Engineering*, vol. 2, special issue1, Dec.2013.

List of Publications

Refereed Papers

- [1] **D. Yu**, J. Zeng, J. Zhao and J. Ning, “A two-stage four-port inverter for renewable energy system integration,” *Proc. IEEE Appl. Power Electron. Conf.*, pp. 3257-3262, Mar. 2019.
- [2] Z. Yang, J. Zeng, **D. Yu**, Z. Zhang and Q. Zhang, “Two-stage power decoupling for a single-phase photovoltaic inverter by controlling the DC-link voltage ripple in the dq frame,” in *Proc. IEEE Appl. Power Electron. Conf.*, pp. 424-429, Mar. 2020

Refereed Conference Proceeding Papers

- [1] **D. Yu**, X. Du, J. Zeng, and Z. Yang, “Control of a Grid-tied Multiport Inverter for a Microgrid with Renewable Energy Sources,” in *Proc. IEEE Energy Conversion Congress and Exposition Conf.*, Oct. 2020, to appear.